APPENDIX B: EXAMPLES

B-1. General

The information in this appendix is provided to assist the designer in understanding certain aspects of performing a nonlinear, incremental structural analysis (NISA). Included are discussions on mesh size and selection, evaluation of cracks and crack potentials, and a parametric study of varying the placing temperature of the concrete. The information presented in this enclosure was taken from the report on the Olmsted project "Nonlinear, Incremental Structural Analysis of Olmsted Locks and Dam, Volume I" ((Garner et al. 1992) listed in Reference section of Appendix A).

B-2. Mesh Size and Selection

a. General. As described in paragraph 5*c*, Appendix A, there are certain restrictions on element size which must be maintained when developing a mesh for a NISA. Considerations must be given for certain restrictions in the heat transfer analysis as well as ensuring that enough elements are present in the model to capture the structural response in the stress analysis, which includes using two rows of elements per lift of concrete and at least two elements through the thickness of any given member. While it is important to adhere to the requirements listed in Appendix A, in some instances it may become necessary to exceed the criteria with respect to the number of elements and the size of elements to reduce computing time and the amount of output data. The following discussion provides insight into the mesh development for the NISA which was performed on the typical chamber monolith of the Olmsted Locks.

b. Olmsted chamber monolith. Figure B-1 is a sectional elevation of a typical chamber monolith of the Olmsted Locks and the finite element (FE) mesh used in the NISA study of the monolith. The Olmsted project implemented the innovative concept of a W-frame lock which has a common wall between the two lock chambers and is a variation on the more common U-frame type lock. The dimensions of the monolith are typical for a massive reinforced concrete structure.

(1) Heat transfer analysis considerations. Due to the algorithm used in ABAQUS for performing the heat transfer analysis, a criterion for the element size is given in paragraph 5*c*(5), Appendix A. Based on this equation, a minimum timestep of one-quarter day and the other necessary data from the Olmsted project, the maximum element size which may be used in the heat transfer analysis is 26.9 in. As can be seen in Figure B-1, the majority of the mesh adheres to the criterion given in paragraph 5*c*(5), Appendix A. It is only toward the center of the slab that the criteria is exceeded and it is exceeded only in the horizontal direction. Truman, Petruska, and Ferhi (1992) (listed in Reference section of Appendix A) show that it is acceptable to exceed the criteria in the direction perpendicular to heat flow. Since the direction of heat flow in the slab, away from the walls, is vertical, then it is acceptable to increase the element size above the criterion in the horizontal direction.

(2) Stress analysis considerations. As stated in paragraph 5*c*, Appendix A, conventional FE modeling techniques should be adhered to when developing a mesh for a NISA. In addition, paragraph 5*c*(2) discusses some specific areas where these techniques can be supplemented. As can be seen in Figure B-1, the mesh for the Olmsted chamber monolith follows these suggested guidelines. There are at least two elements in every lift and at least two elements through the thickness of every member.

c. Additional considerations. While the chamber monolith from the Olmsted project followed the guidelines for mesh size and selection as outlined in Appendix A, following these guidelines may not always be practical, particularly in three-dimensional analyses. Any deviation from the criteria and guidelines outlined in paragraph 5*c*, Appendix A, should be evaluated on a case-by-case basis. Parametric studies may be appropriate to justify exceeding the restrictions in some cases, where in other cases past experience and engineering judgement can be used.

B-3. Evaluation of Cracks and Cracking Potentials

a. General. Due to the low tensile capacity of concrete, cracking is likely to occur in any concrete structure. While cracking can be expected on massive concrete structures, it is the size and location of

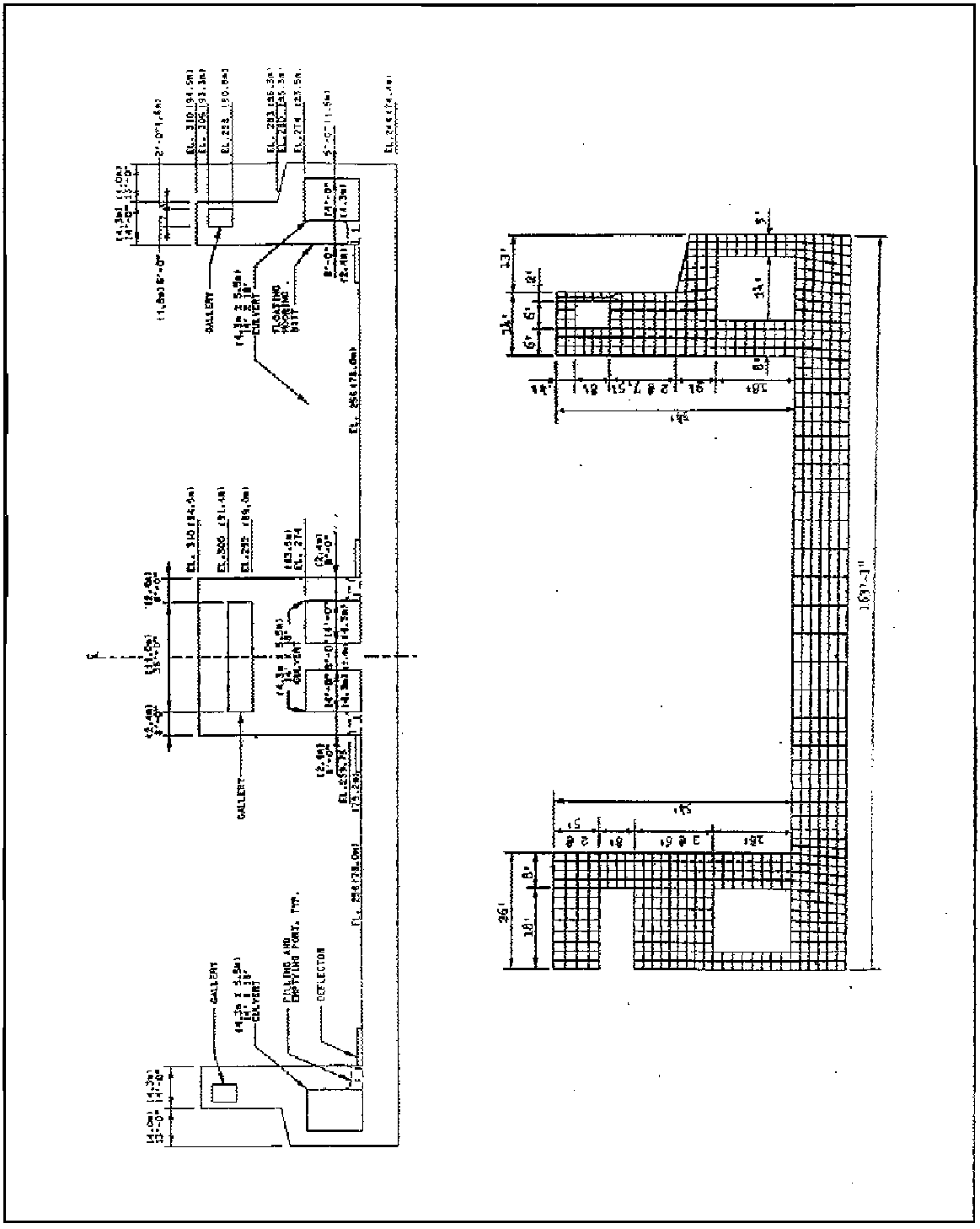

Figure B-1. Sectional elevation of a typical chamber monolith at Olmsted Locks and the NISA finite element mesh

the cracks that form which are important as well as areas where there is a high potential for cracking. If a NISA shows that only a few integration points exceed the cracking criteria (discussed in Annex 2, Appendix A) and the analysis shows that the cracking has stopped, then measures to reduce the cracking may not be necessary, particularly if reinforcing is present. If it is shown though that the cracking extends through the depth of a member, then consideration must be given to making changes to reduce the cracking regardless of the fact that reinforcing is present. This section will discuss cracking potentials and crack plots and how to use this information. The chamber monolith shown in Figure B-1 is used for this presentation. It should be noted that the cracking criteria was reduced by one-half in the following analyses so that cracking would occur.

b. Crack plots.

(1) Figures B-2 through B-5 are crack plots of the middle wall and one-half of the chamber and Figures B-6 and B-7 are crack plots of the land wall and one-half of the chamber. As can be seen in Figure B-2, no cracks have formed at 81.5 days (time of the analysis is designated by the AMP parameter located at the top of the plot). Figure B-3 is a plot at 85.75 days and as can be seen, an integration point above the top left corner of the culvert has cracked. It can be seen by looking at Figures B-4 and B-5 that the crack does not extend beyond this initial cracking. Such a crack would typically not require taking measures to eliminate the crack, particularly for a reinforced structure.

(2) Figure B-4 is a plot at 143 days and an integration point has cracked at the lower left hand corner of the culvert and six integration points have cracked approximately one-third of the way across the slab. As can be seen in Figure B-5, 20 days after the condition shown in Figure B-4, the crack at the bottom corner of the culvert has not grown, but the crack in the slab has extended further into the slab. The crack as shown in Figure B-5 is as far as the crack advanced. As with the crack at the top of the culvert, no additional steps should be needed at the bottom of the culvert. The crack in the slab may need to be evaluated further. The design team should evaluate a crack such as the one seen in Figure B-5. Then, based on the load causing the crack and the stresses in the reinforcing, a decision should be made as to whether steps should be taken to reduce or eliminate the crack. Since the crack seen in the slab in Figure B-5 was created due to ambient conditions and the stresses in the reinforcing are low, it would be reasonable to allow the construction parameters to remain unchanged.

(3) Figure B-6 shows the cracking which has begun to occur on the land wall half of the slab. Three integration points have cracked initially and do not extend beyond the top lift. Figure B-7 shows the final crack pattern in this portion of the slab at day 183 and only one additional integration point has cracked. As with the cracking which occurred in the other portion of the slab, the crack indicated by the plots does not continue to propagate. If stresses in the reinforcing are evaluated, they are low, so as before, changes in the construction parameters to reduce or eliminate the cracking shown do not appear to be necessary.

c. Crack potential plots.

(1) Figures B-8 through B-14 are crack potential contour plots of the middle wall half of the model, while Figures B-15 through B-18 are crack potential contour plots of the land wall half of the model. The contours shown in these plots provide information about how close to cracking various parts of the structure are in the form of percentages of the cracking criteria, i.e., a 50 percent contour indicates that the level of stress and strain is one-half the cracking criteria. These plots can be used to identify areas that are near the cracking level.

(2) Figure B-8 is a crack potential plot of the left half of the model at day 81.5 which is just a few days prior to the crack occurring at the top left corner of the culvert. As can be seen in the figure, high cracking potentials are developing at this corner. An enlarged view of the culvert is shown in Figure B-9 and in this figure it can be seen that the potential for cracking at the corner in question is approximately 70 percent. Figure B-10 is the enlarged view of the culvert again, but it is shown at day 85.75, which is the step after the crack has formed at the corner. As can be seen, the cracking potential near the corner has been reduced, and the potential for cracking of 66 percent is occurring more toward the center of the culvert.

(3) Figure B-11 again shows the left half of the model at day 103. The potential for cracking near the top left corner of the culvert continues to build to a level of 88 percent. In addition, the top of the slab

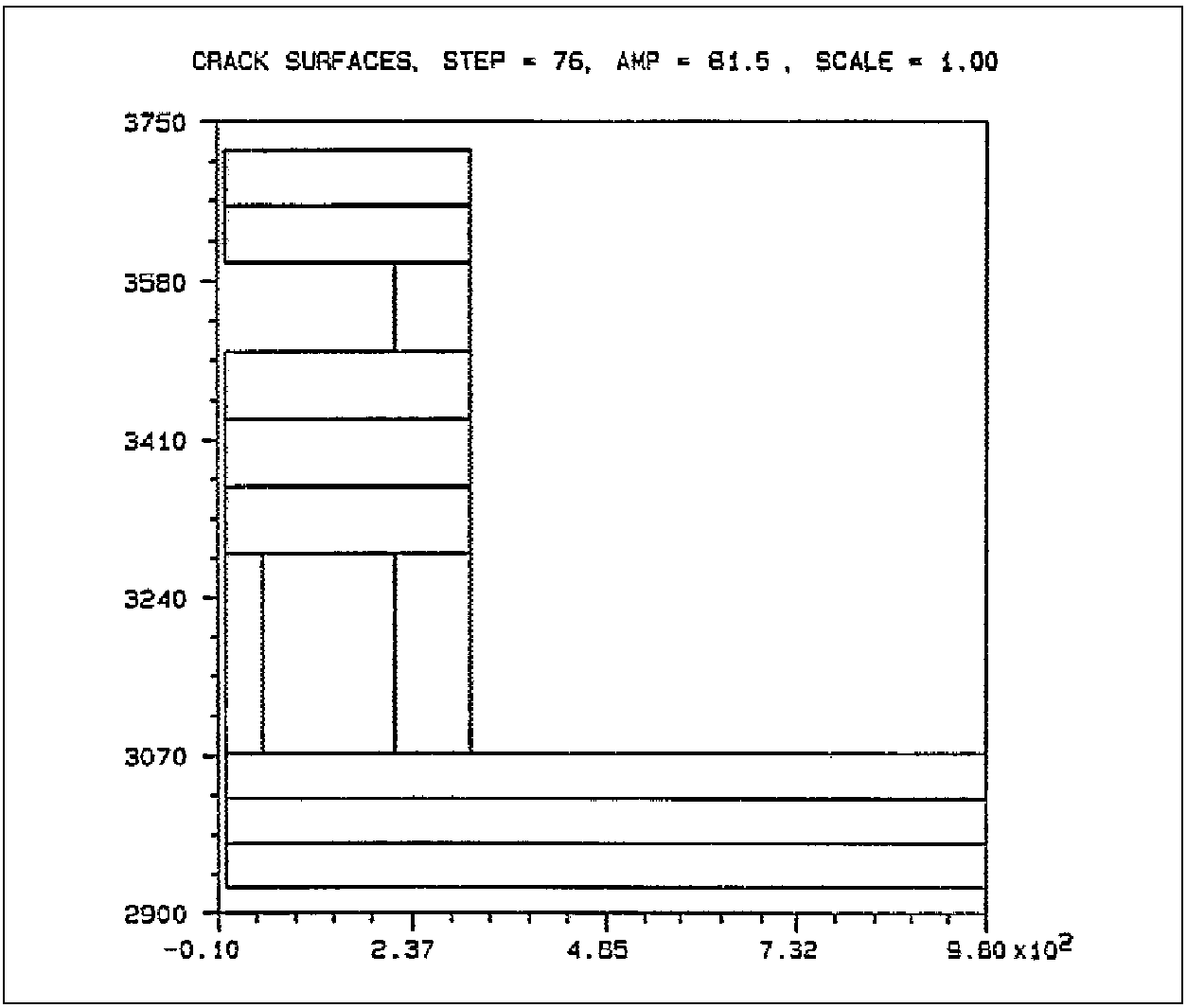

Figure B-2. Crack plot at day 81.5 of the middle wall half of the chamber monolith model

has portions which are over 50 percent. Figure B-12 shows contours at day 115 and the potential at the top of the slab has risen to over 70 percent, but the crack potential at the top of the culvert has begun to decrease. In addition, note that a potential of 89 percent exists at the top of the lift above the gallery. This high potential and the crack potential building in the slab are due to ambient condition which is entering the winter season. Figure B-13 is taken at 143 days and is after the cracking in the slab has initiated. The cracked area has reduced potentials near the top of the slab, but a potential of 96 percent remains at the bottom of the top lift. Note to the right of the cracked area, the cracking potential is nearly parallel with the top surface indicating a uniform level of cracking potential across the top of the slab. Figure B-14 is the cracking potential after all of the cracking has occurred in this portion of the slab. Note that the potentials in the area of the crack are lower than in other areas, but they have not all gone to zero. This is because tensile stresses and strains which may still be present but are not perpendicular to the crack surface continue to be evaluated against the cracking criteria.

(4) Behavior of the right half of the model is similar to the left half as seen in Figure B-15. An area of high potential is building in the top of the slab (68 percent) and also at the corner of the culvert, although the potentials at the culvert corner are much lower than those observed on the left half of the model. Both of these potentials continue to build,

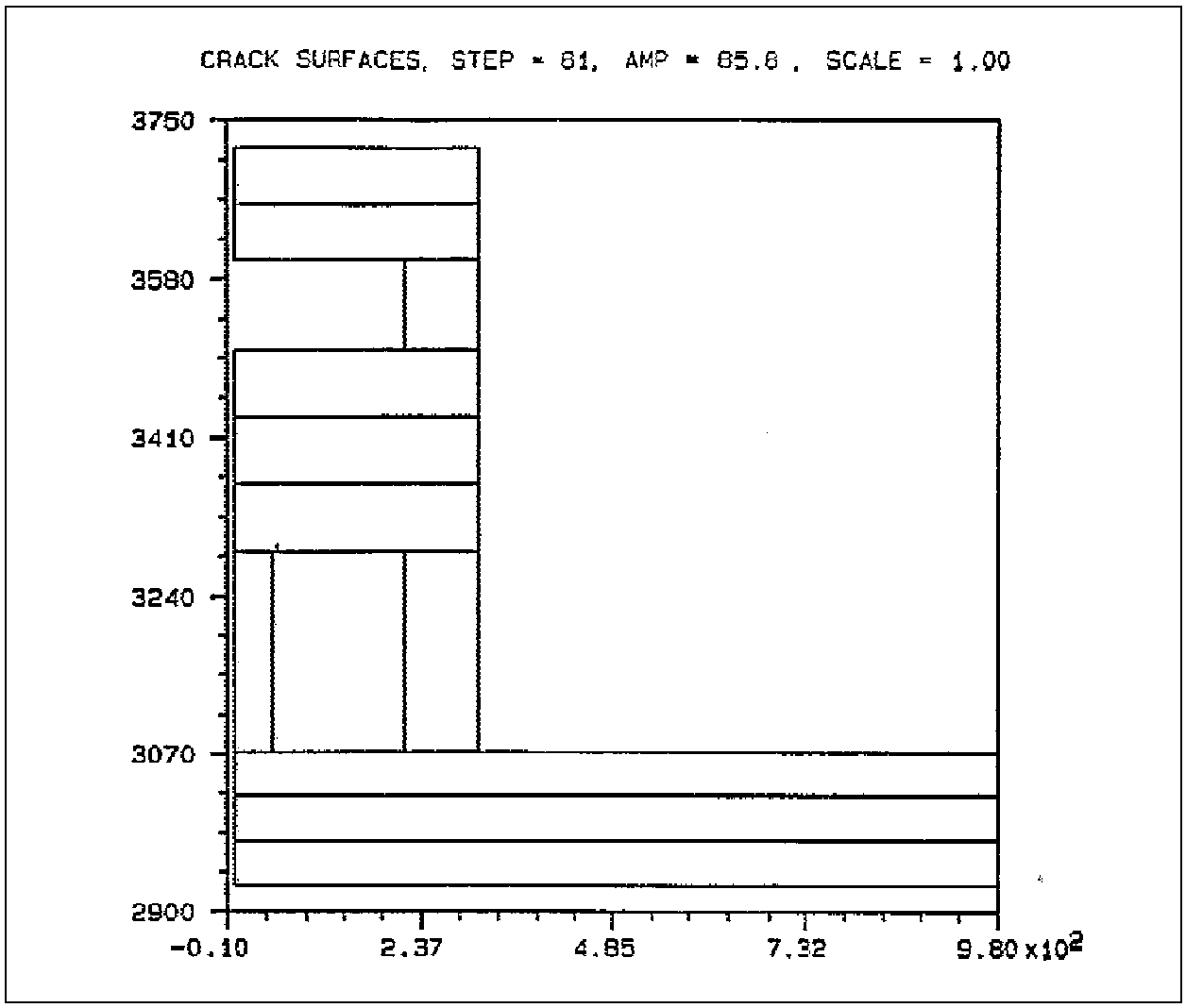

Figure B-3. Crack plot at day 85.75 of the middle wall half of the chamber monolith model

particularly in the slab as seen in Figure B-16 (day 143) where a potential of 96 percent occurs. Figure B-17 is a plot at day 163 after the initial cracking in this portion of the slab has occurred. The location of the crack is obvious from the reduced area of potential. Also, the point where the next integration point will crack can be seen in the figure by the designation of the 98 percent cracking potential. The potentials after all of the cracking has occurred are shown in Figure B-18 and are similar to what was observed in the left half of the model.

B-4. Placing Temperature Parametric Study

a. General. One of the parametric studies performed during the course of the Olmsted project's NISA study was an evaluation of concrete placing temperatures. It is a regular practice in mass concrete construction to reduce the temperature of the concrete when it is placed as a means of reducing the maximum temperature that the concrete will reach since lowering the maximum temperature can reduce thermal stresses in the concrete. The initial assumption

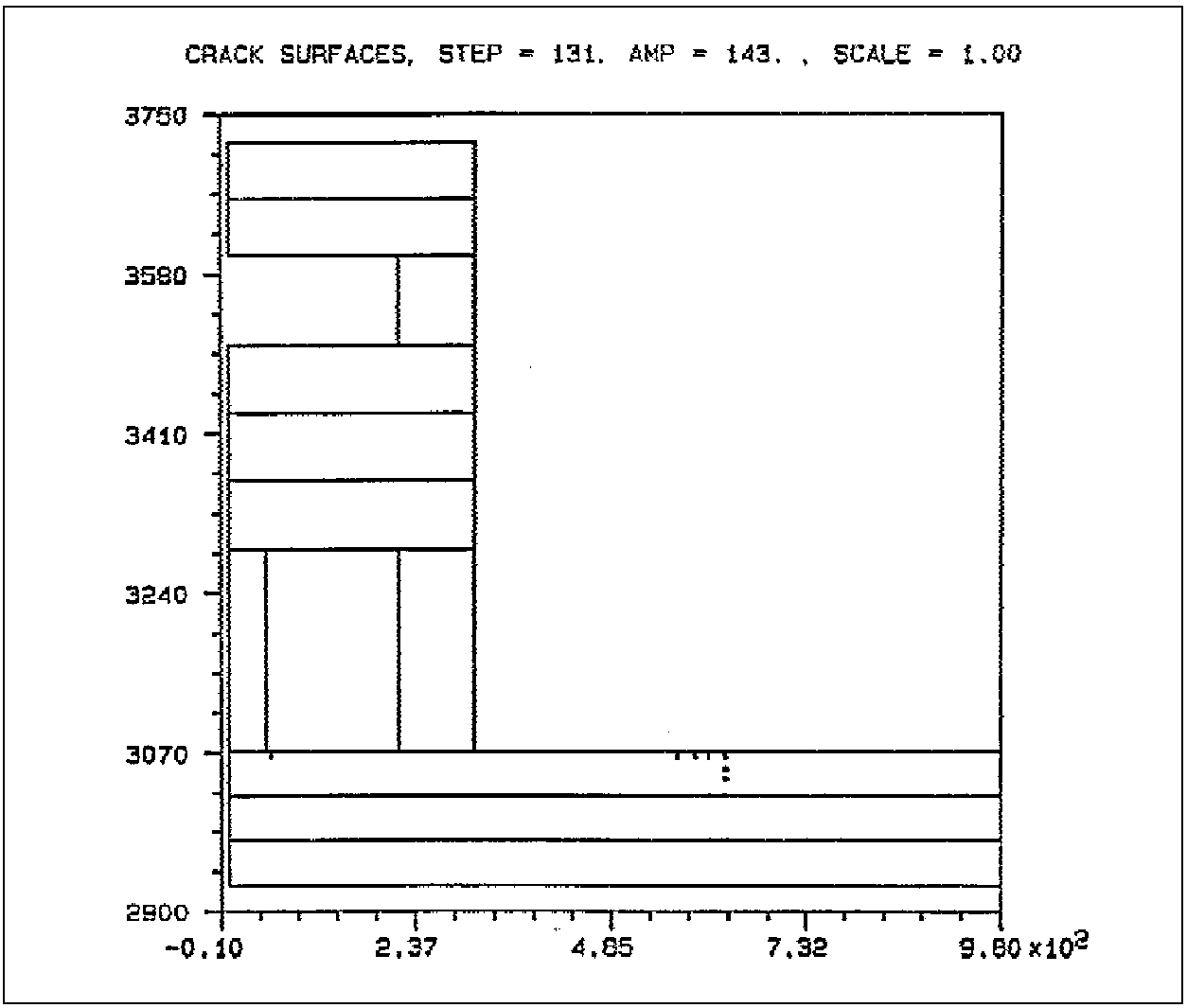

Figure B-4. Crack plot at day 143 of the middle wall half of the chamber monolith model

for the concrete placing temperature for lock construction was 60 °F. Since cooling the concrete to this temperature during the summer months would require adding ice in place of water or including liquid nitrogen to the mixture, it was determined that higher placing temperatures should be evaluated to determine if costs associated with cooling the concrete could be reduced. Two additional analyses were performed. One analysis used a placing temperature of 70 °F, and the other used a placing temperature equivalent to the ambient temperature at the time the lift was placed. The study was performed on the chamber monolith of the Olmsted project as shown in Figure B-1.

b. Analysis results.

(1) Temperature results. The results of the heat transfer analysis should first be evaluated for the three cases under consideration. Time-history temperature plots are presented for three points in the slab in Figures B-19 through B-21. The initial observation on all three plots is that a noticeable difference exists when the concrete is first placed due to the different placing temperatures for each case, but at 300 days very little difference exists between the three analyses. It should also be noted that while the general shape of the curves in all three figures follow the shape of the ambient temperature curve

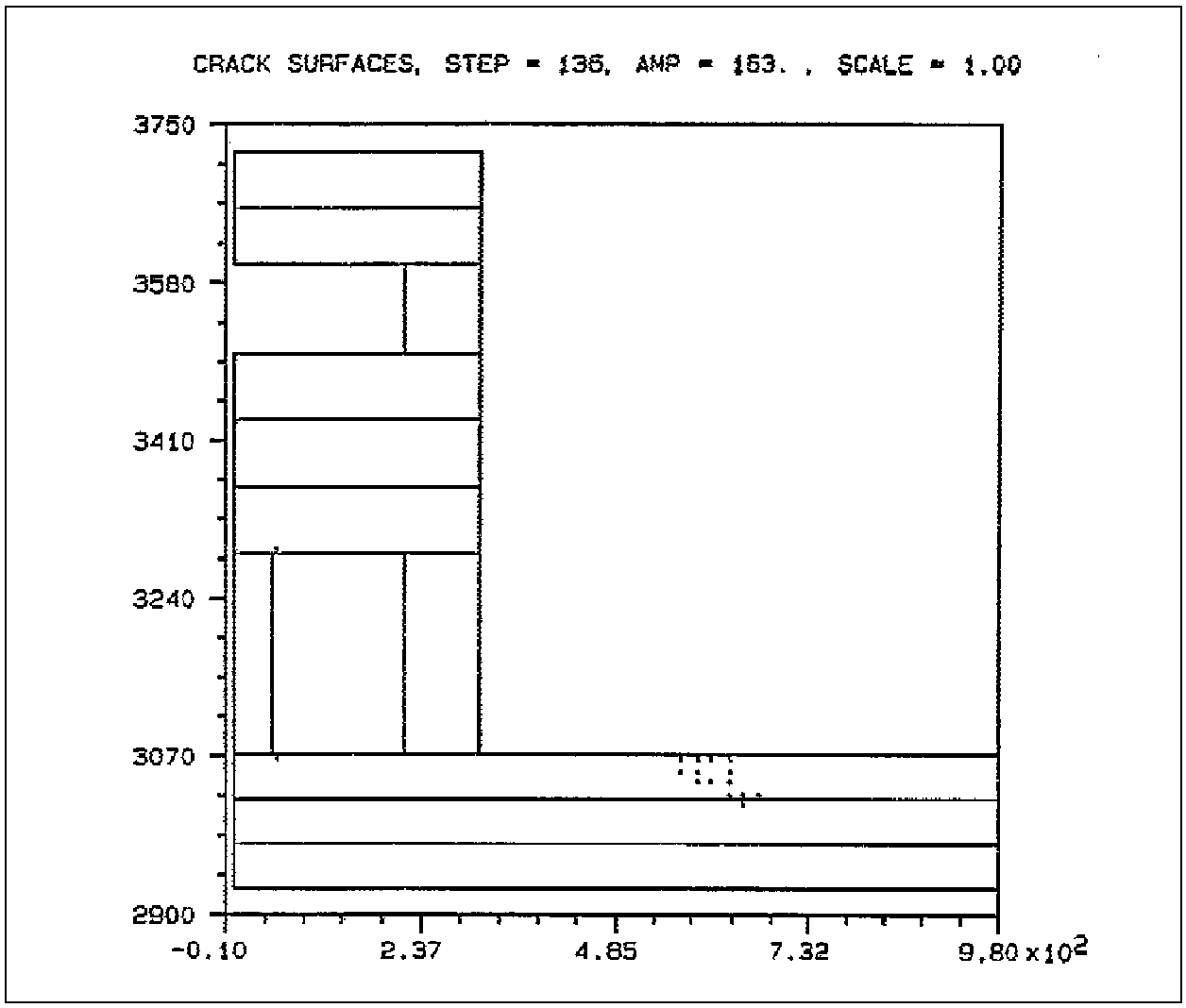

Figure B-5. Crack plot at day 163 of the middle wall half of the chamber monolith model

(designated in the plots by "Extreme Ambient"), node 3371 near the top of the slab follows the ambient much more closely than the other two curves. If the plots from the three figures were superimposed upon one another, a substantial temperature gradient would occur from the top to the bottom of the slab at approximately day 200.

(2) Stress results. Plots of stress used in evaluating the results are shown Figures B-22 through B-26. Figure B-22 is a time-history plot of the horizontal stress at the point of maximum stress in the chamber monolith. As mentioned previously, in the past it has been assumed that a higher placing temperature would create the worse condition, but Figure B-22 shows that this is not the case in this instance. The maximum stress for the 60 °F placing temperature case is approximately 80 psi higher than the maximum stress at this point for the ambient placing temperature case. While these results do not match conventional understanding from analysis of mass concrete structures, there is a logical explanation. The results shown in Figure B-22 are essentially a surface effect as shown in the stress distribution plot in Figure B-23. Surface effects cause the stress to be lower for the ambient placing temperature, but at other points through the slab thickness this is not necessarily the case. A time history at the second

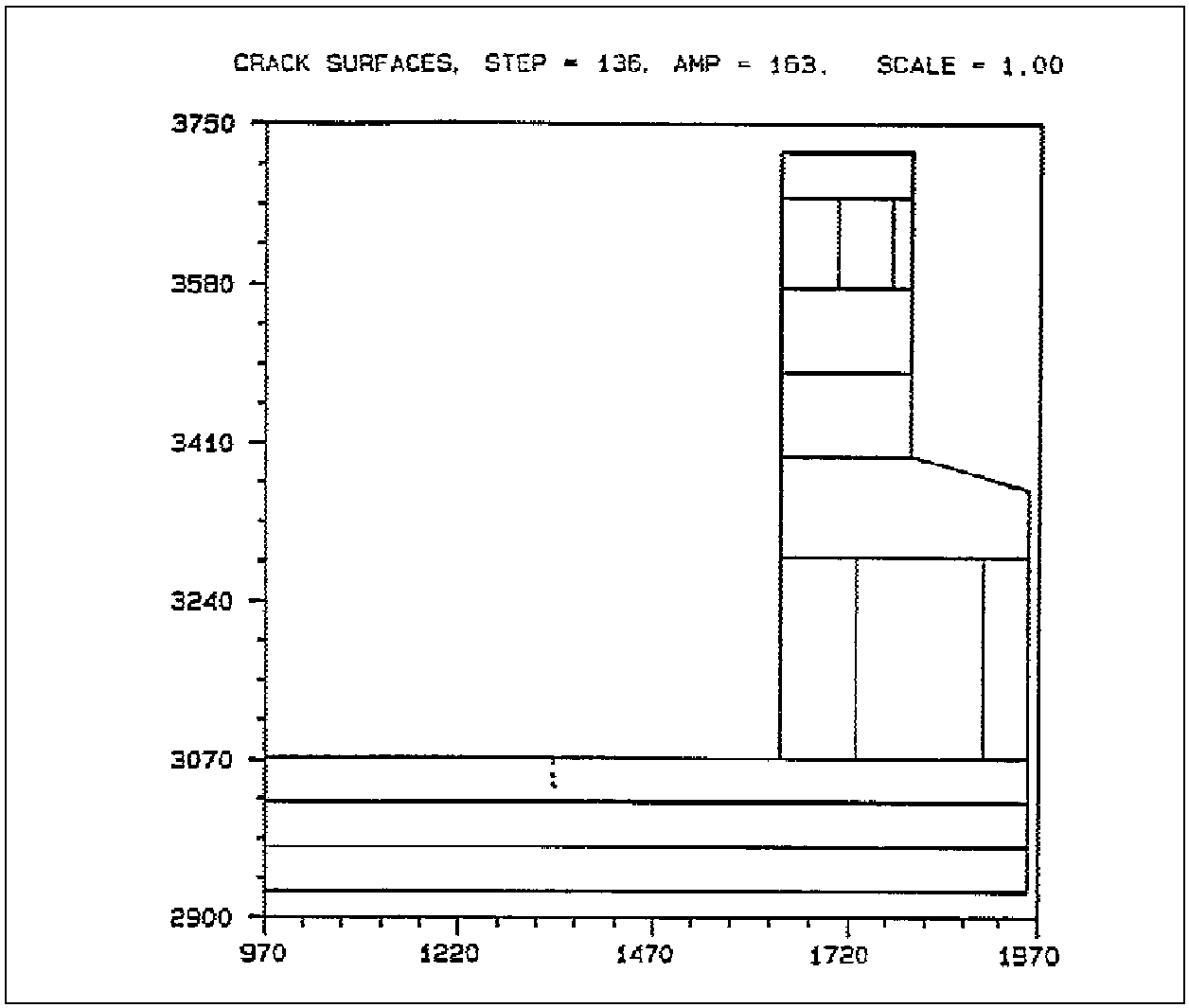

Figure B-6. Crack plot at day 163 of the middle wall half of the chamber monolith model

point from the surface (Figure B-24) shows how the ambient placing scheme has become the more critical of the three cases.

(a) The reason for the behavior exhibited at the top integration point of the slab can be explained if the beginning of the time history is looked at more closely as shown in Figure B-25. As can be seen, the initial stress history of the three cases shows that the ambient placement case produces tensile stresses almost immediately while the other two cases go into compression first. It is at these early times that the highest rate of creep is occurring. Therefore, tension at early times is being relieved for the ambient placement case, while compression is being relieved for the other cases. Since this is a time-history analysis and the stiffness matrix is reformulated with each step based on strain state of the previous step, the relief of stresses occurring has an impact on the results at later times in the analyses, hence the lower stresses for the ambient placement case at day 200.

(b) Finally, Figure B-26 shows a time history of the maximum principal stress at a point in the wall. For this point the ambient placement case controls, but the stresses are relatively low and therefore are not a major concern.

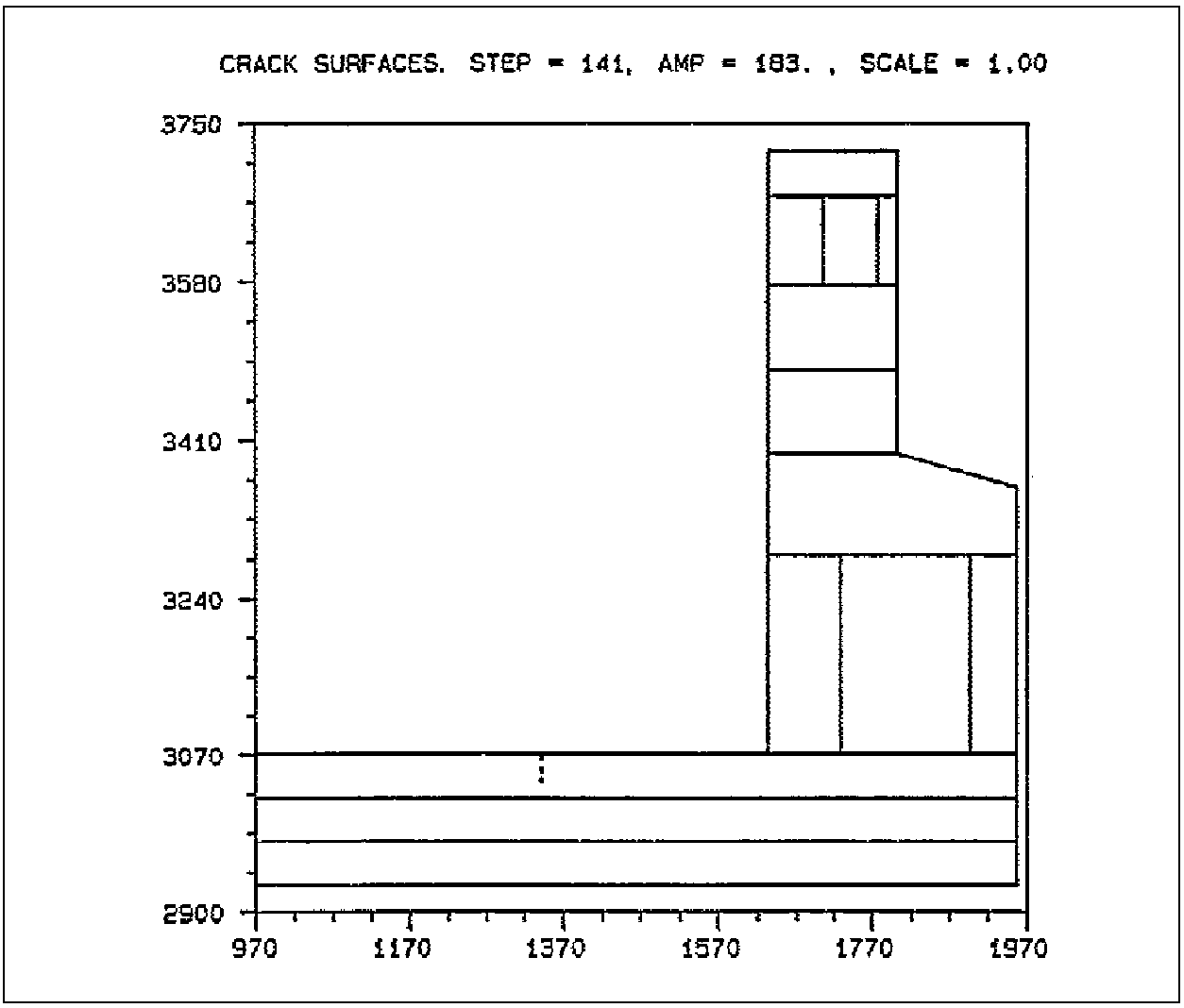

Figure B-7. Crack plot at day 183 of the land wall half of the chamber monolith model

c. Conclusion. Based on the results of the analyses, a conclusion could be drawn that the ambient placement condition was acceptable and could be used during construction for these types of monoliths. Based on the results of the analyses combined with experience of engineers from Headquarters, U.S. Army Corps of Engineers; U.S. Army Engineer Division, Ohio River; U.S. Army Engineer District, Louisville; and the U.S. Army Engineer Waterways Experiment Station, a decision was made to specify a maximum placing temperature of 75 °F.

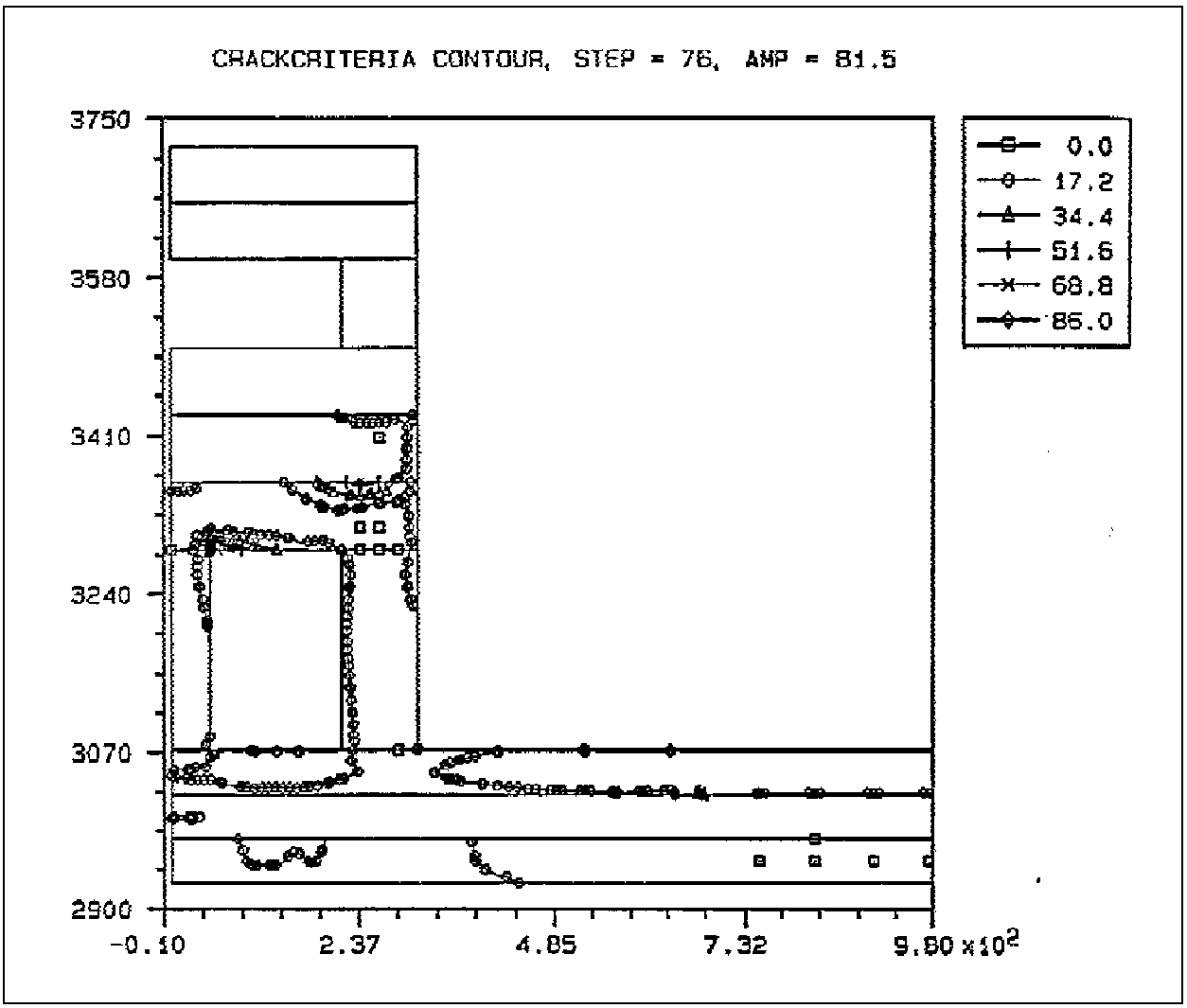

Figure B-8. Crack potentials at day 81.5 of the middle wall half of the chamber monolith model

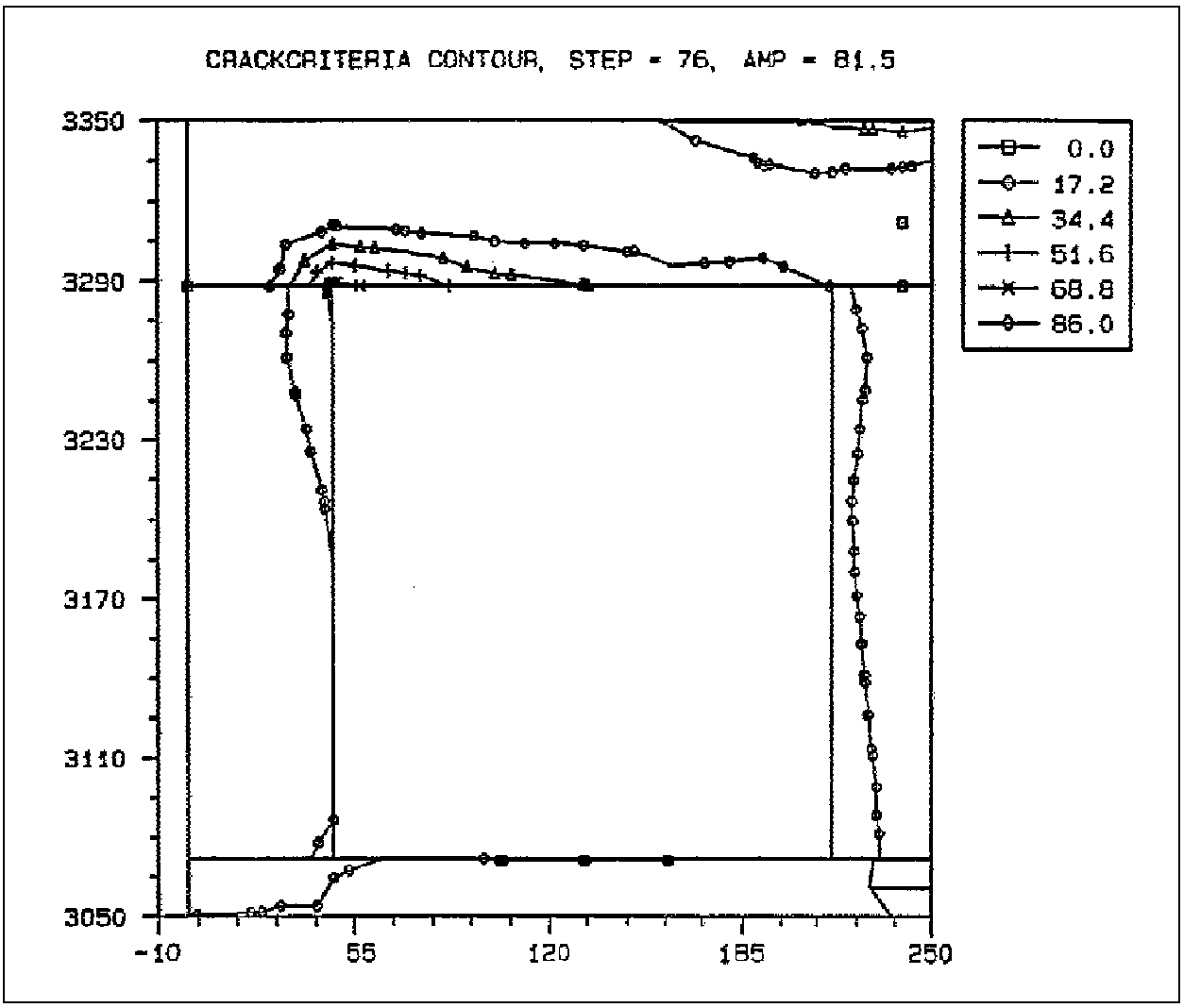

Figure B-9. Enlarged view of crack potentials from Figure B-8 around the culvert at day 81.5

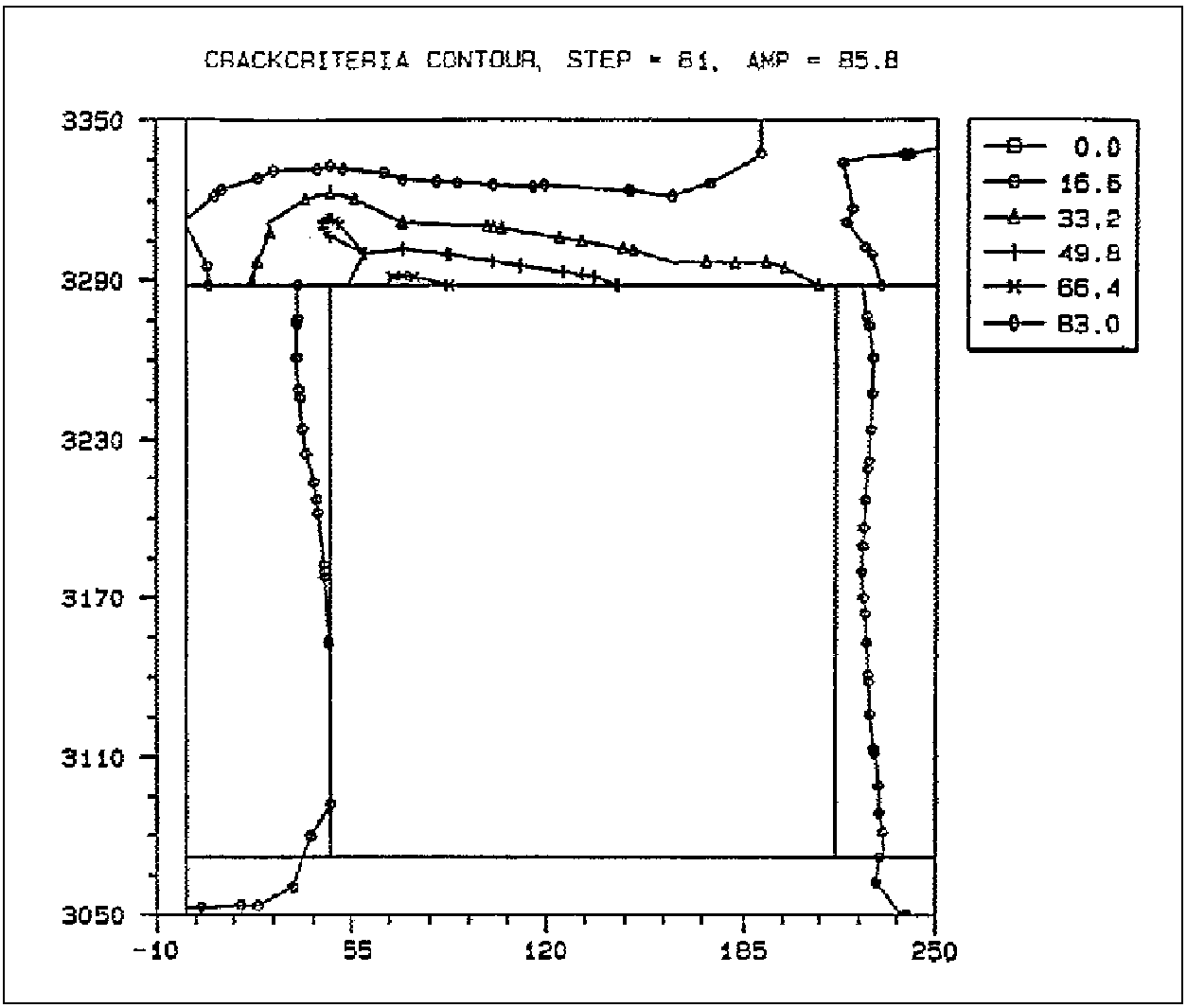

Figure B-10. Enlarged view of crack potentials from Figure B-8 around the culvert at day 85.75

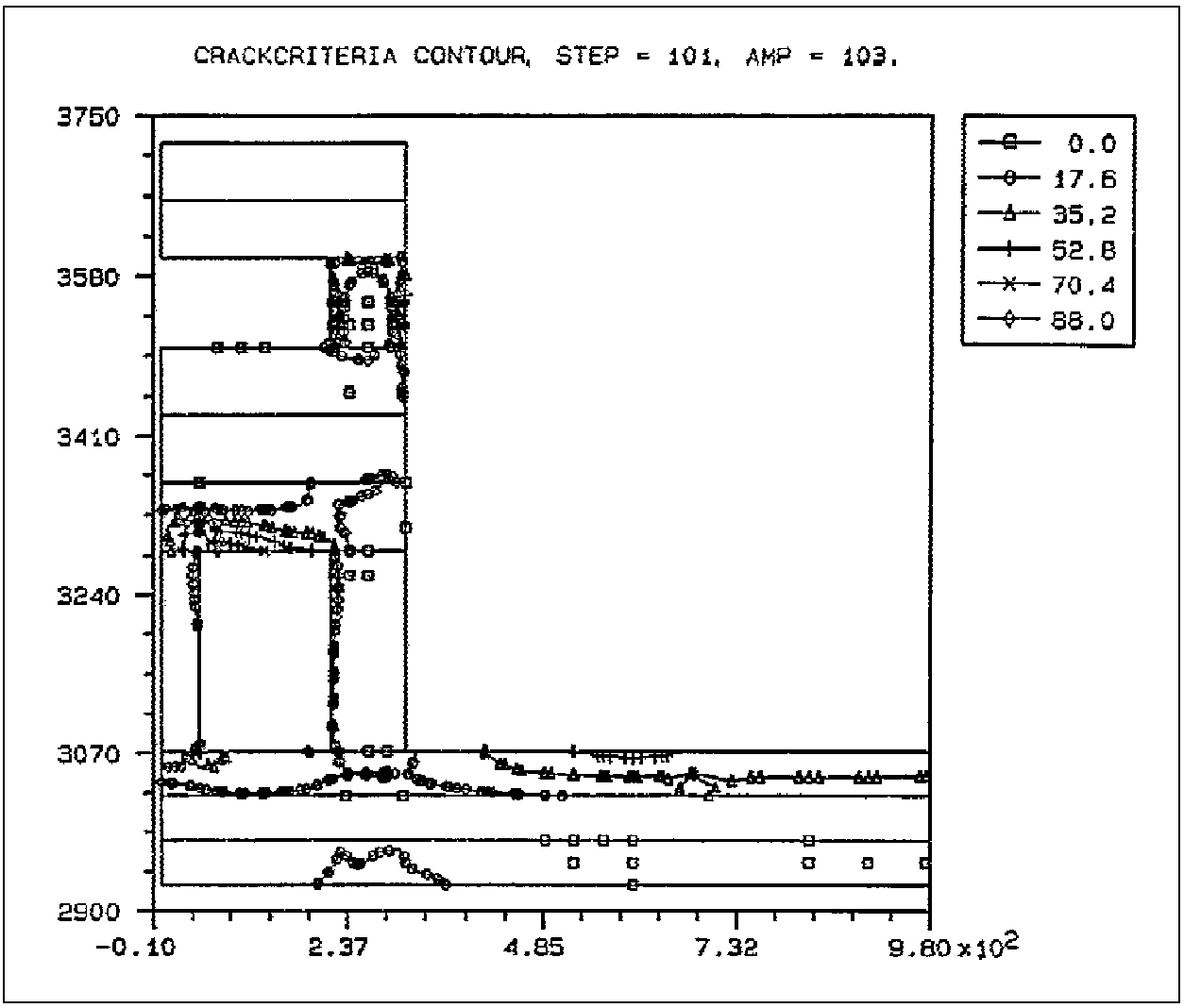

Figure B-11. Crack potentials at day 103 of the middle wall half of the chamber monolith model

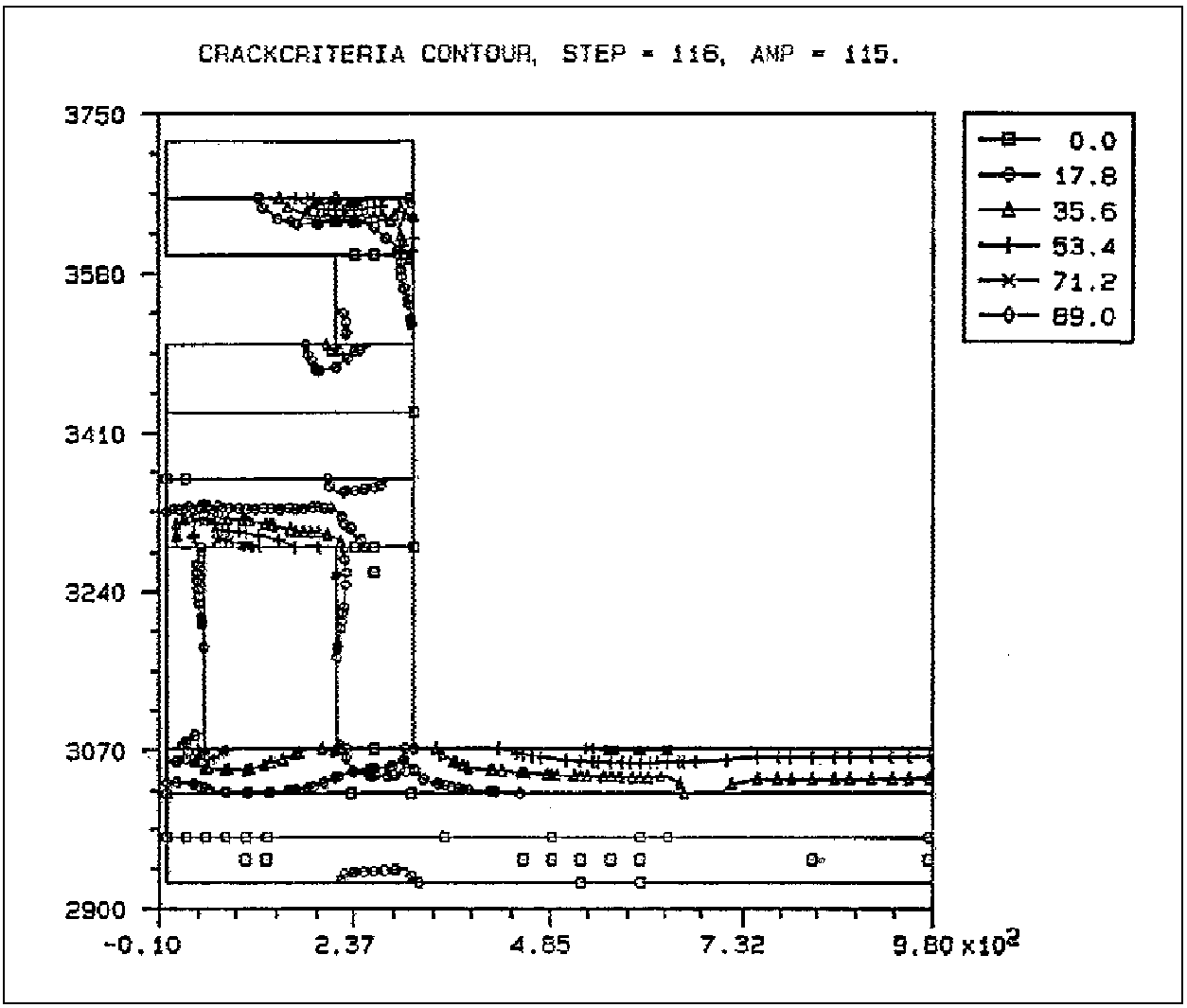

Figure B-12. Crack potentials at day 115 of the middle wall half of the chamber monolith model

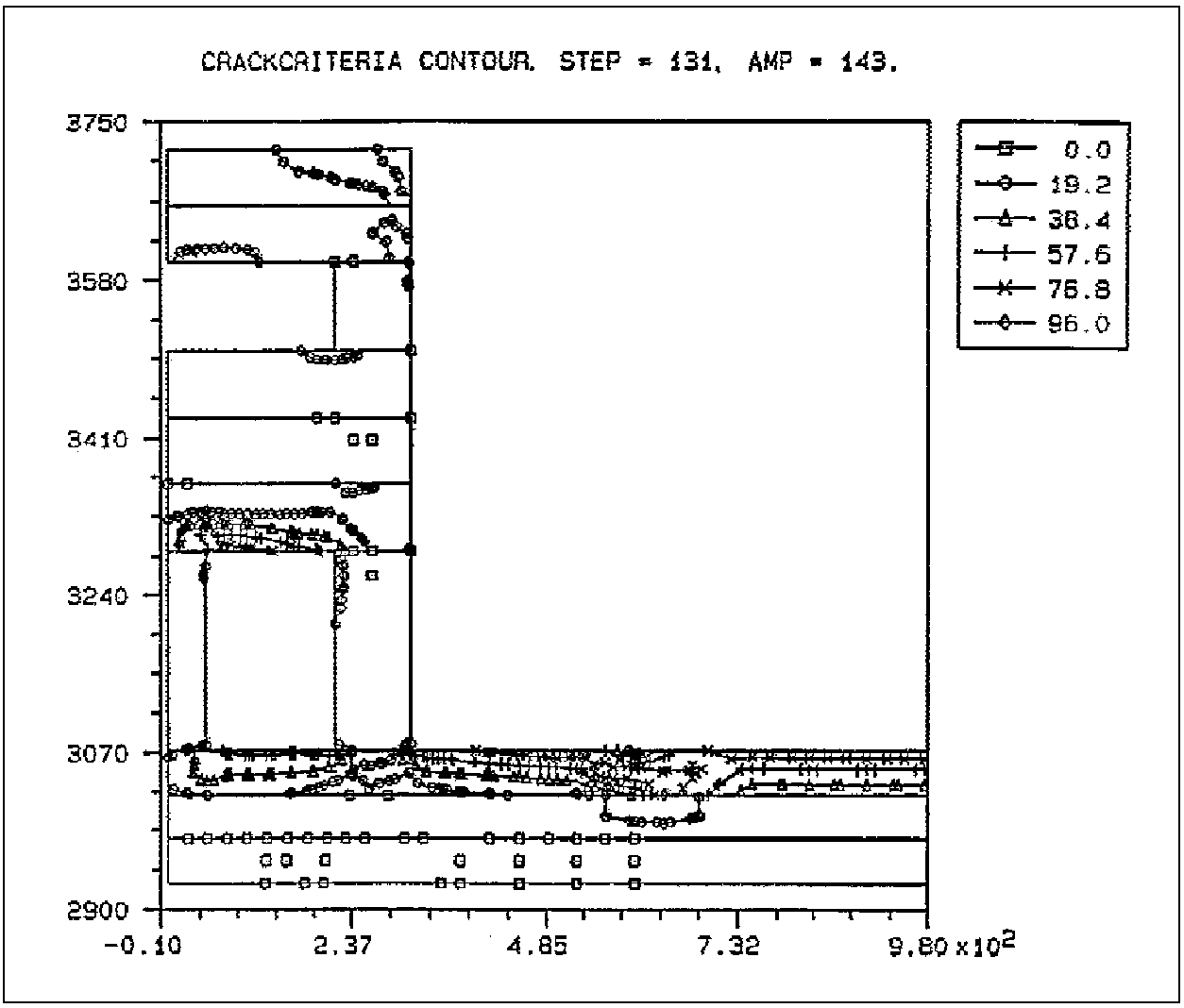

Figure B-13. Crack potentials at day 143 of the middle wall half of the chamber monolith model

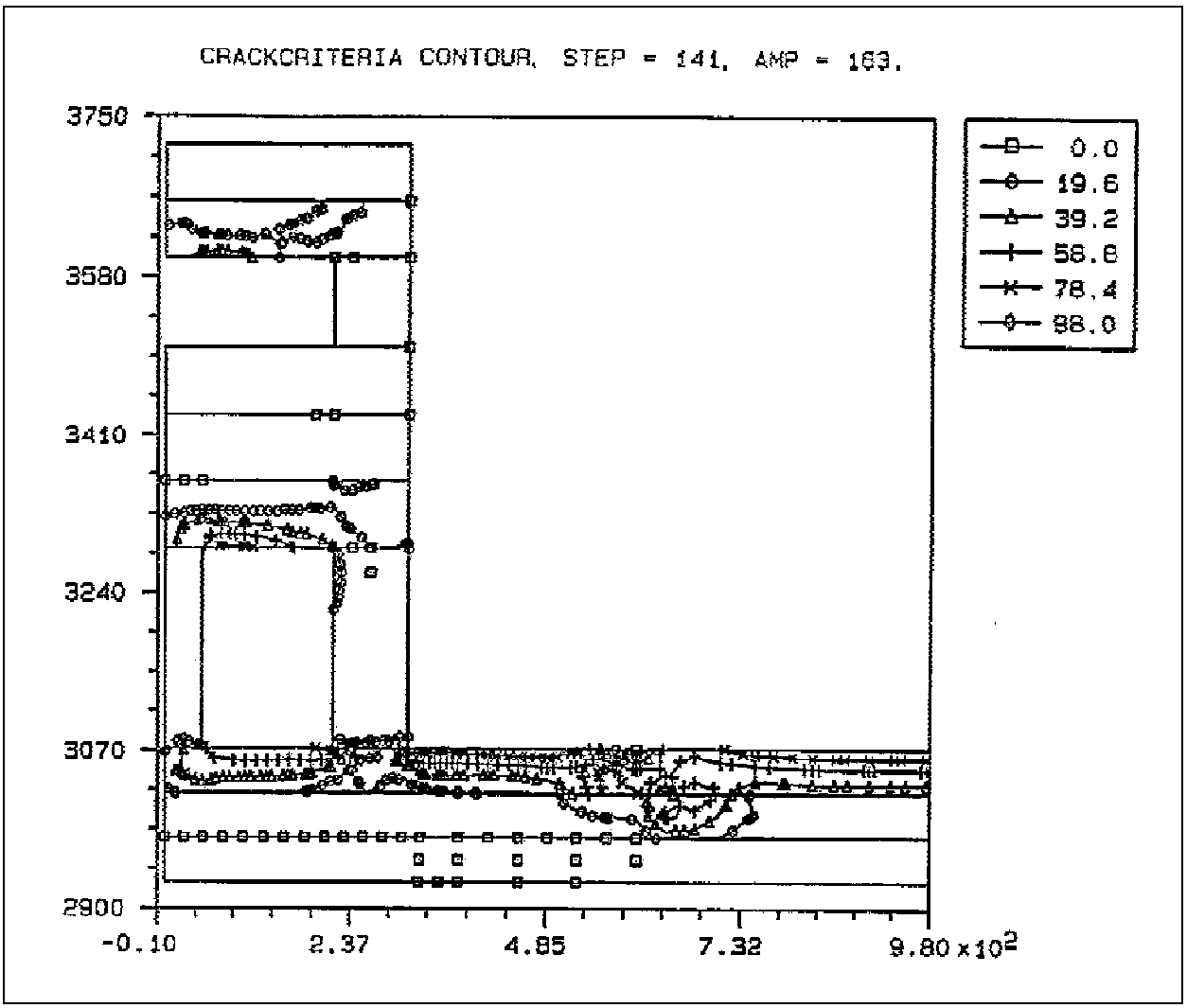

Figure B-14. Crack potentials at day 183 of the middle wall half of the chamber monolith model

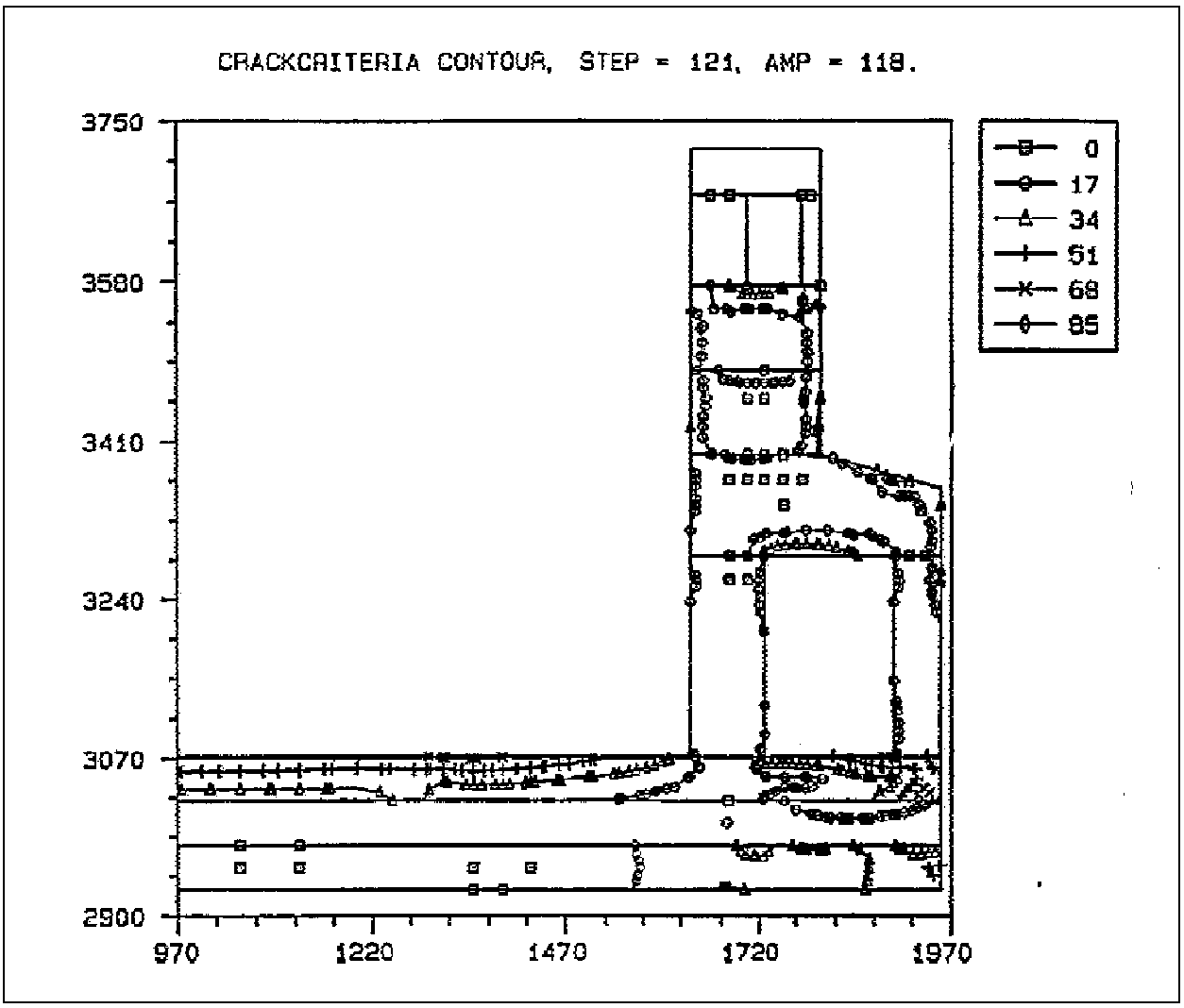

Figure B-15. Crack potentials at day 118 of the land wall half of the chamber monolith model

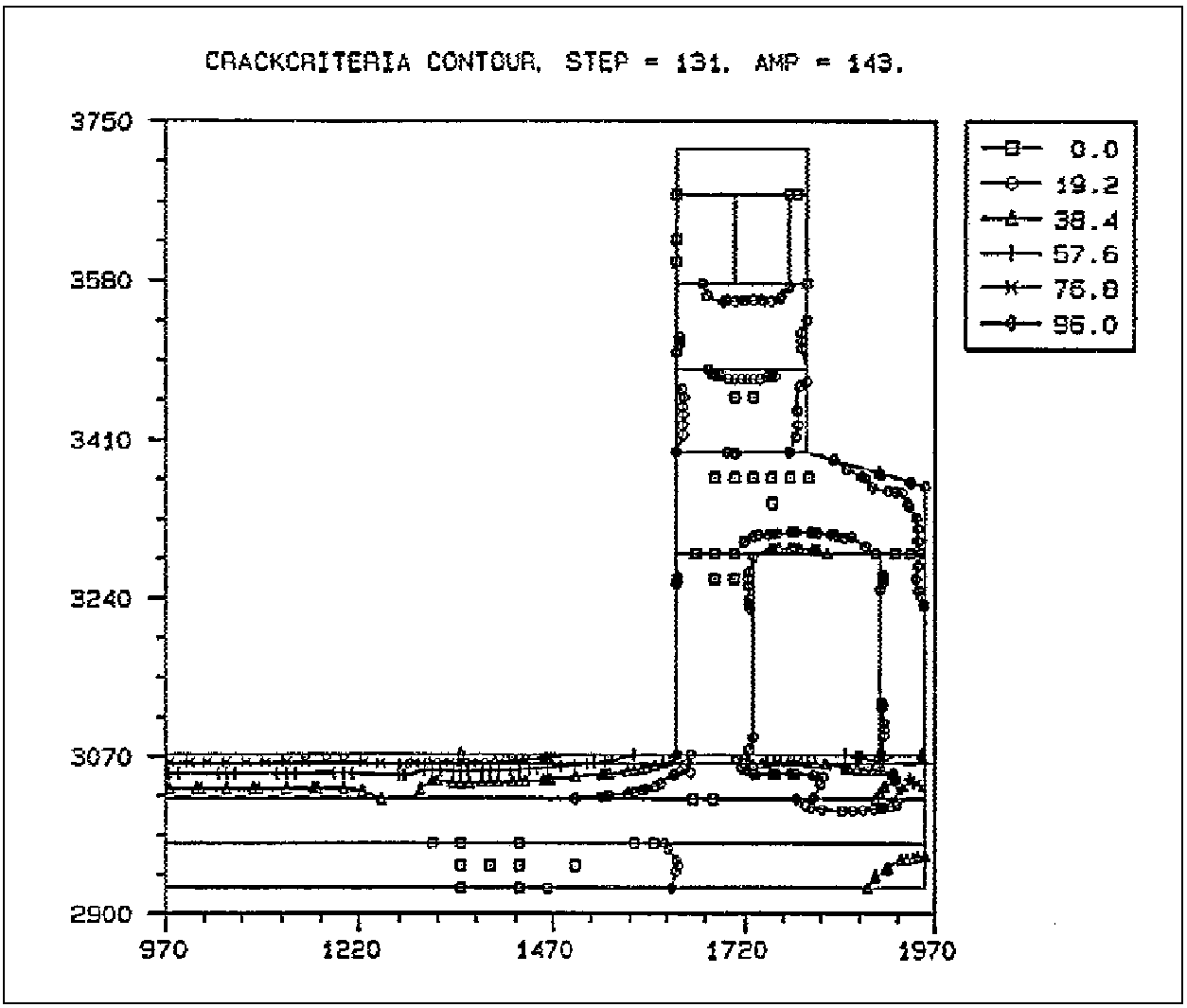

Figure B-16. Crack potentials at day 143 of the land wall half of the chamber monolith model

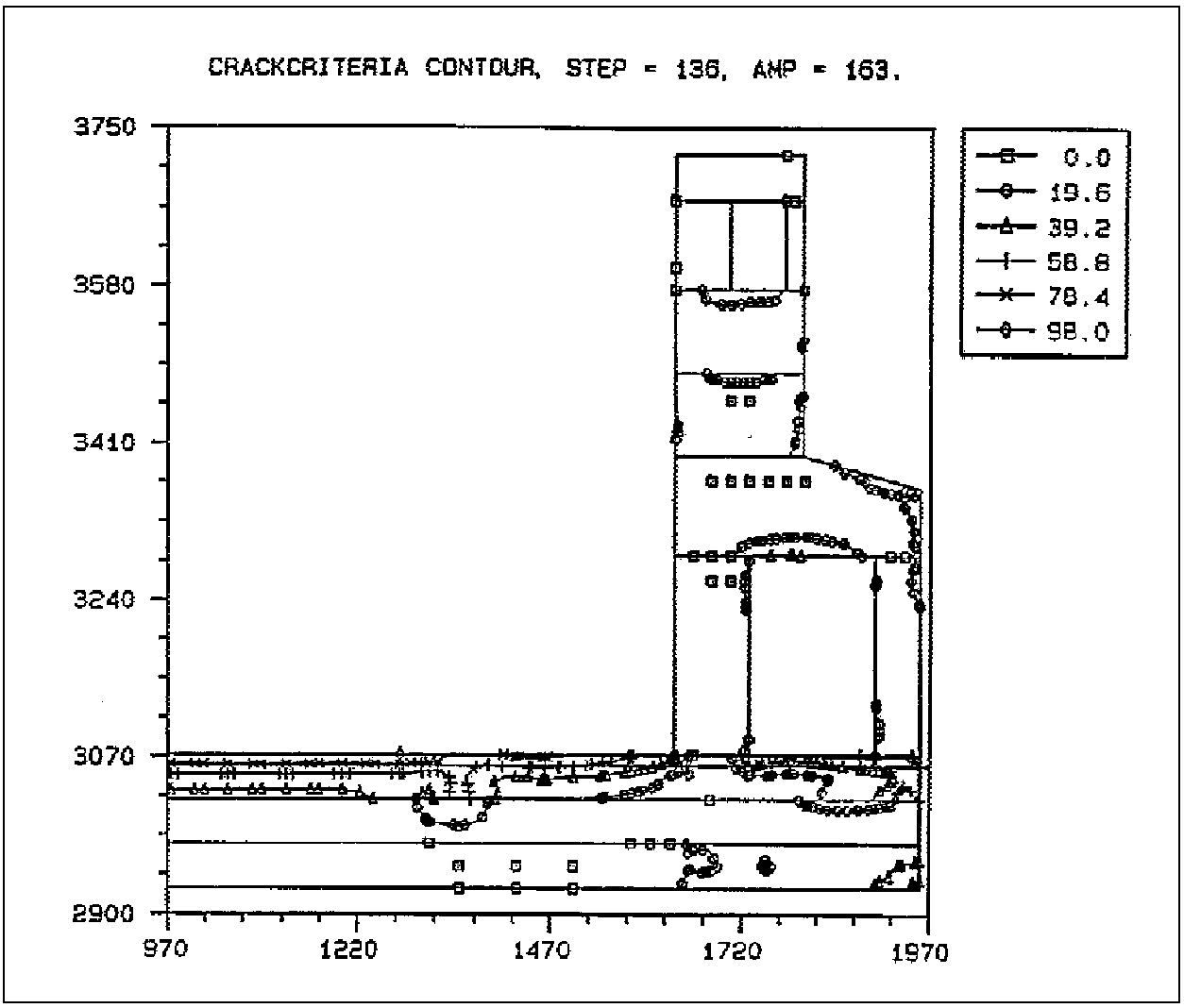

Figure B-17. Crack potentials at day 163 of the land wall half of the chamber monolith model

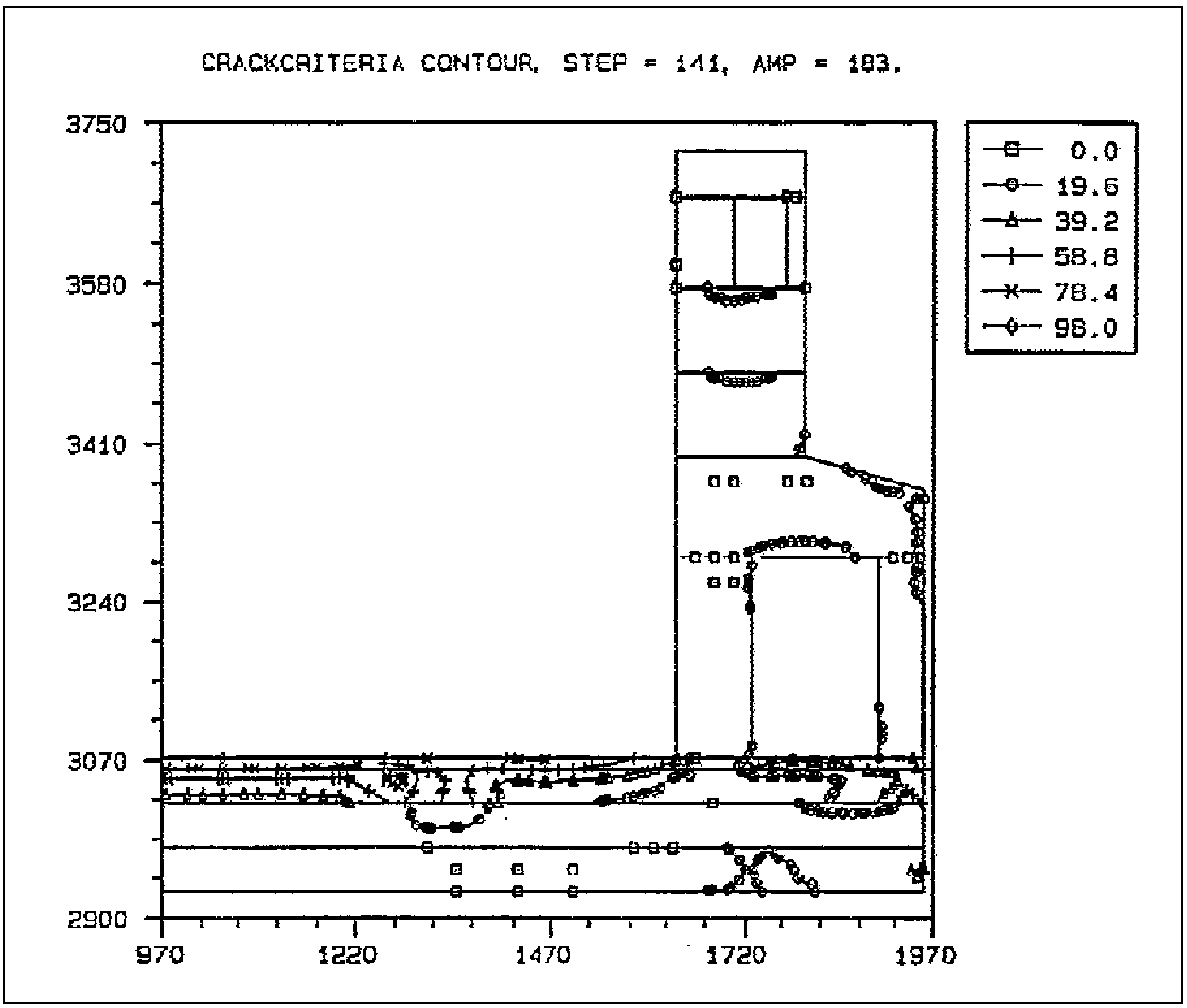

Figure B-18. Crack potentials at day 183 of the land wall half of the chamber monolith model

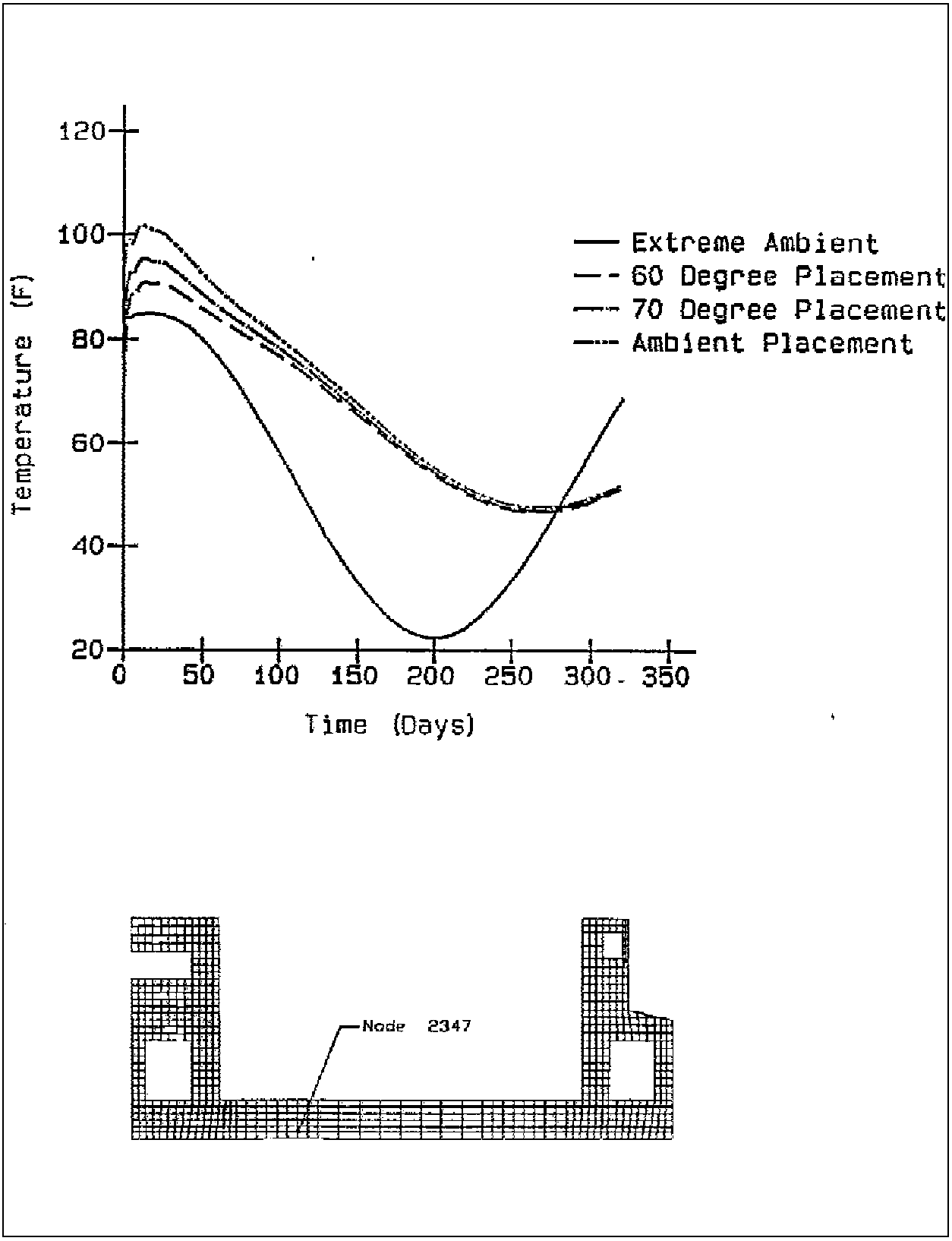

Figure B-19. Temperature time history at node 2347 of the chamber monolith model

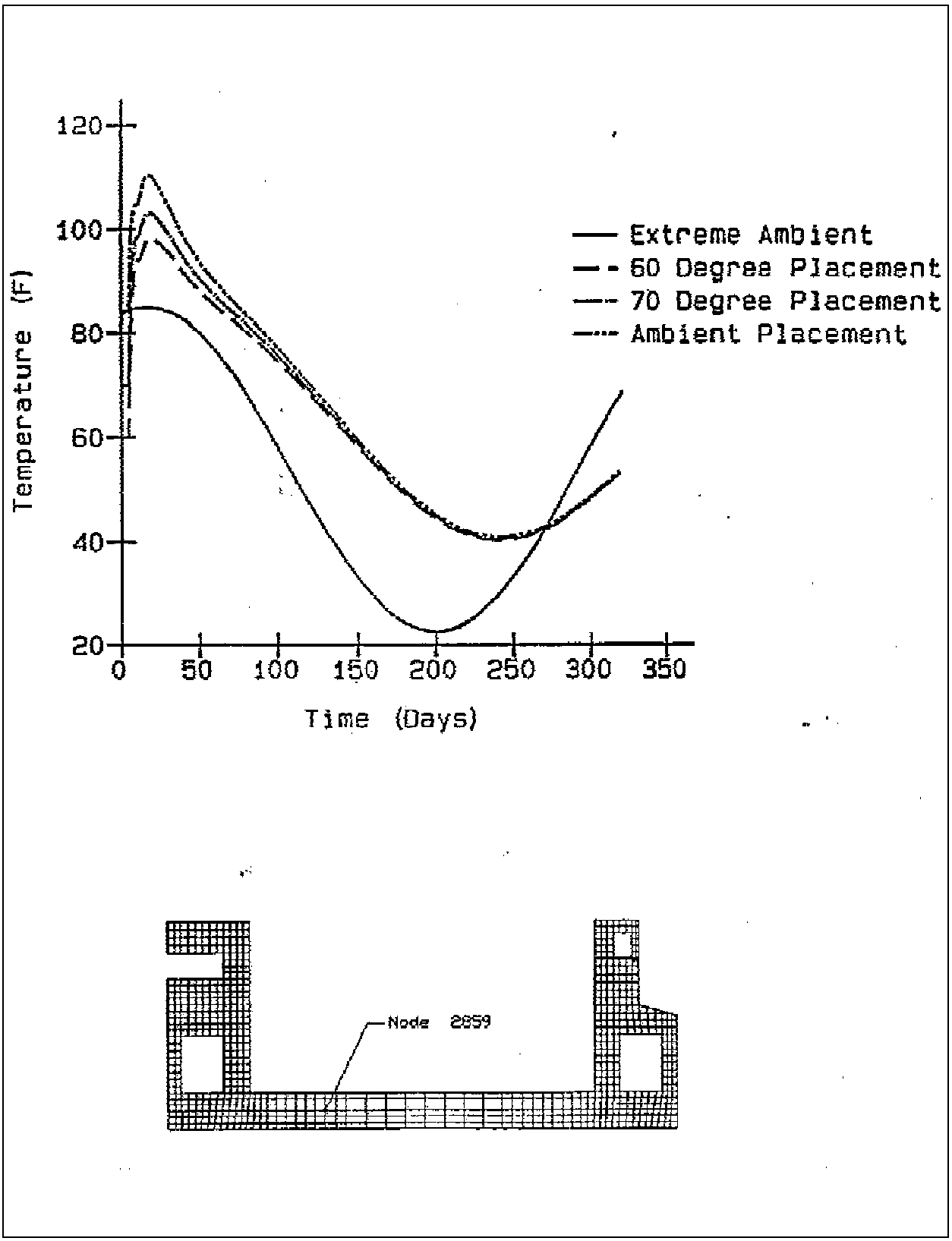

Figure B-20. Temperature time history at node 2859 of the chamber monolith model

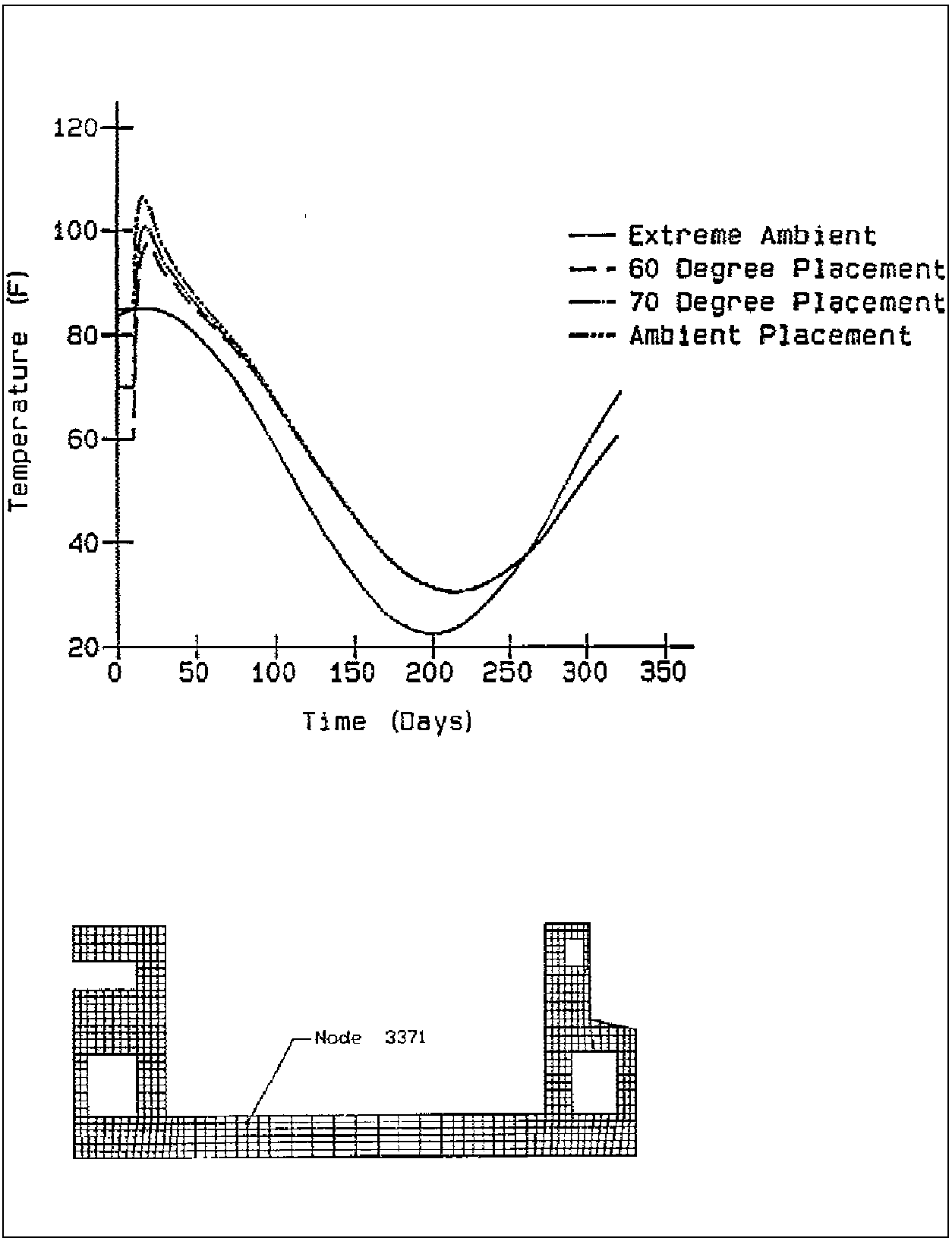

Figure B-21. Temperature time history at node 3371 of the chamber monolith model

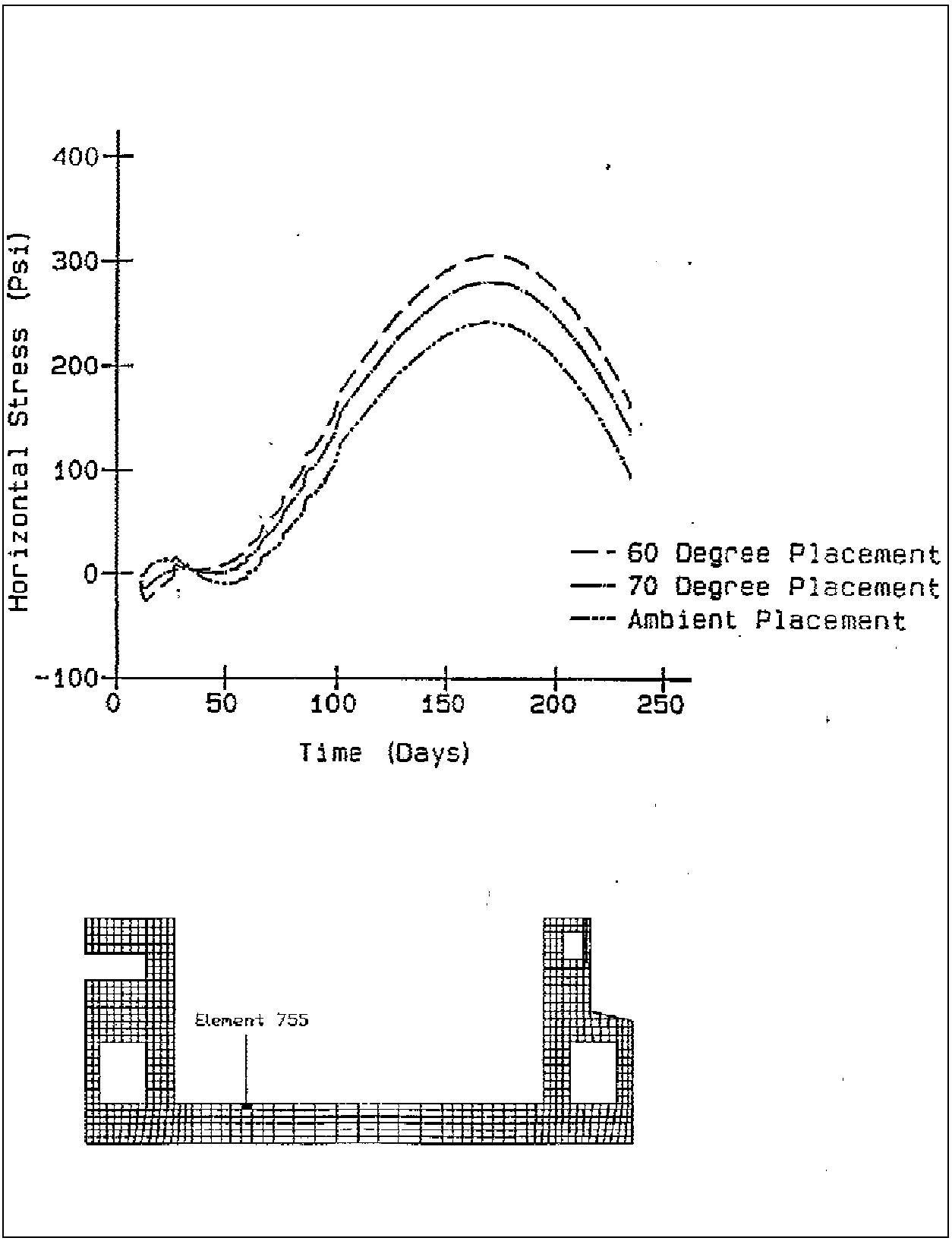

Figure B-22. Horizontal stress time history at integration point 4 of element 755 of the chamber monolith model

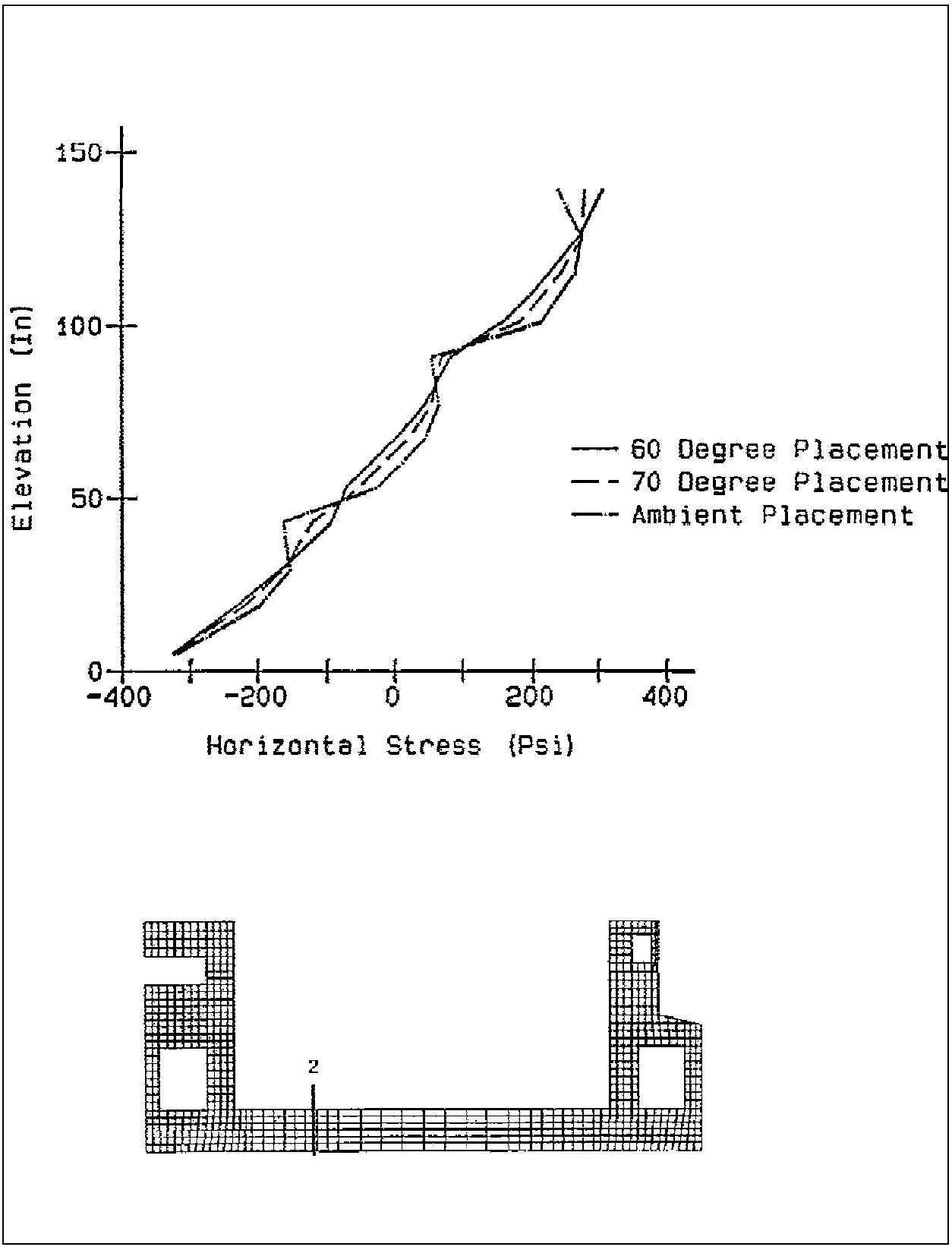

Figure B-23. Stress distribution of horizontal stress through the slab at day 177.5

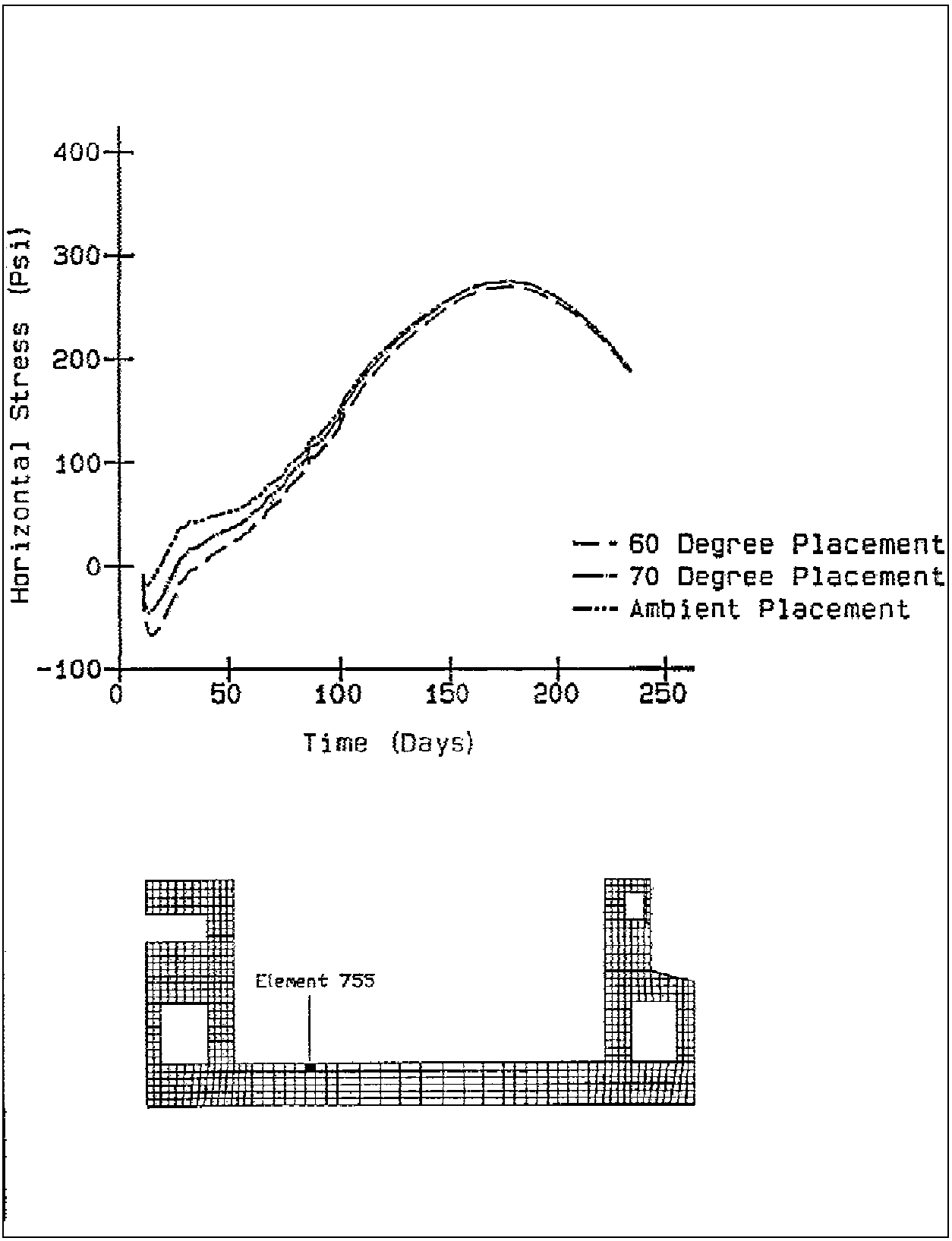

Figure B-24. Horizontal stress time history at integration point 2 of element 755 of the chamber monolith model

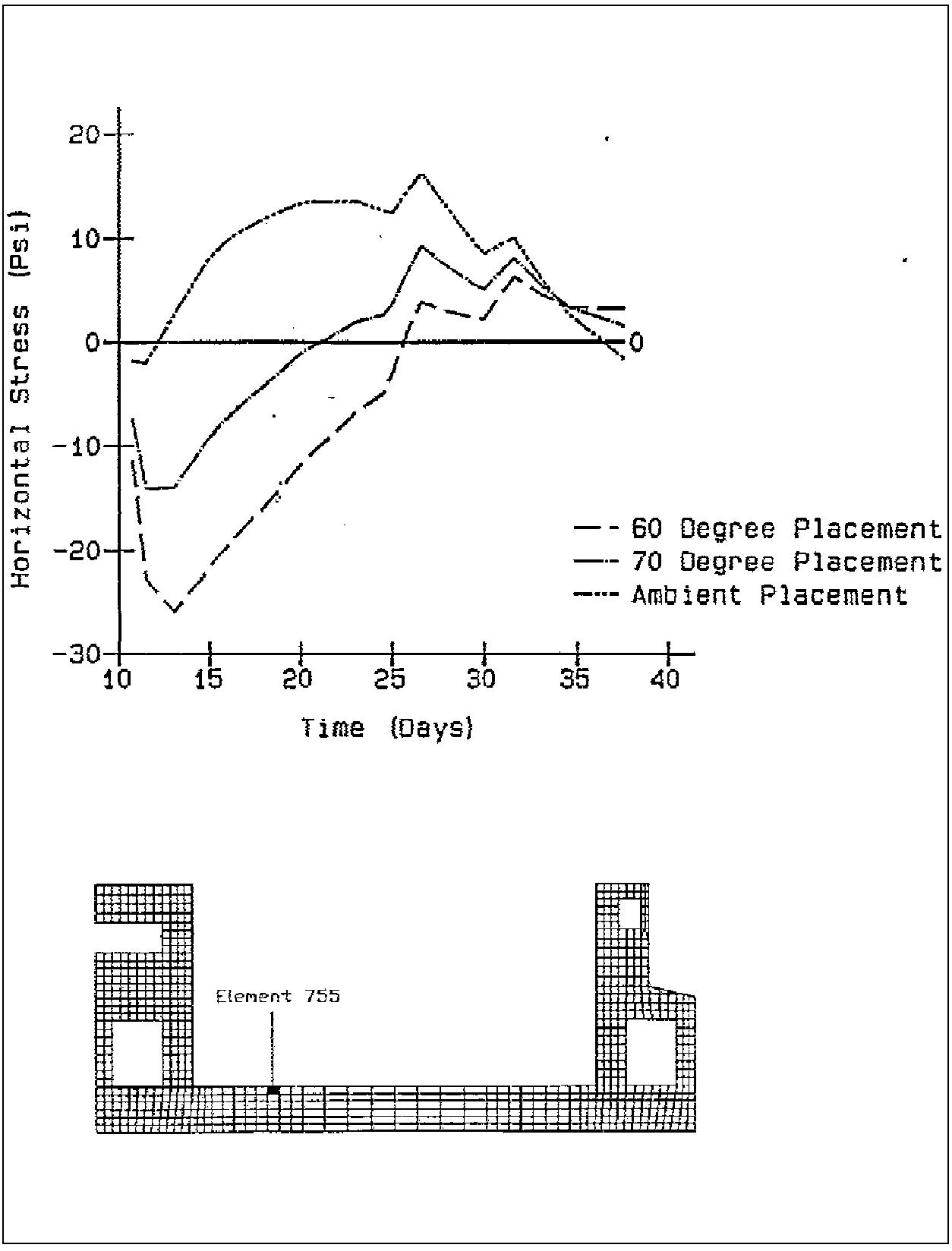

Figure B-25. Horizontal stress time history for the first 40 days at integration point 4 of element 755

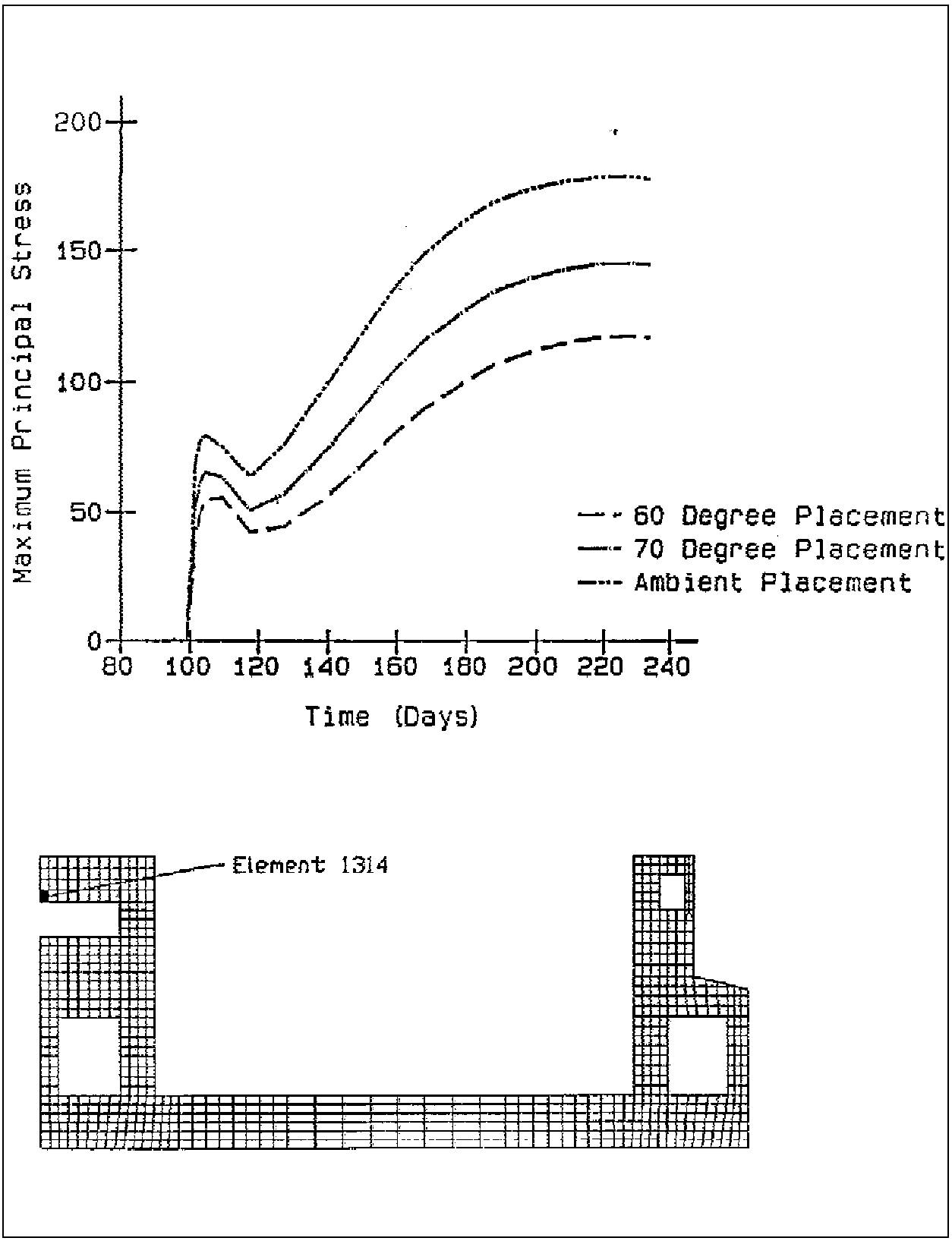

Figure B-26. Maximum principal stress time history at integration point 3 of element 1314 of the chamber monolith model